



Discovery of 5-(or 6)-benzoxazoles and oxazolo[4,5-*b*]pyridines as novel candidate antitumor agents targeting hTopo II α

Esin Karatas^{a,1}, Egemen Foto^{b,1}, Tugba Ertan-Bolelli^{a,2}, Gozde Yalcin-Ozkat^{c,d,2}, Serap Yilmaz^{e,2}, Sanaz Ataei^c, Fatma Zilifdar^f, Ilkay Yildiz^{a,*}

^a Ankara University, Faculty of Pharmacy, Department of Pharmaceutical Chemistry, Ankara, Turkey

^b Necmettin Erbakan University, Faculty of Science, Department of Biotechnology, Konya, Turkey

^c Ankara University, Biotechnology Institute, Ofef0 Yenimahalle, Ankara, Turkey

^d Recep Tayyip Erdogan University, Faculty of Engineering, Bioengineering Department, Rize, Turkey

^e Trakya University, Faculty of Pharmacy, Department of Pharmaceutical Chemistry, Edirne, Turkey

^f Selcuk University Faculty of Science, Department of Biochemistry, Konya, Turkey

ARTICLE INFO

Keywords:

Benzoxazoles
Oxazolo[4,5-*b*]pyridines
Topoisomerase I and II α inhibition
Antitumor
Molecular docking
Molecular dynamic simulation

ABSTRACT

Discovery of novel anticancer drugs which have low toxicity and high activity is very significant area in anti-cancer drug research and development. One of the important targets for cancer treatment research is topoisomerase enzymes. In order to make a contribution to this field, we have designed and synthesized some 5(or 6)-nitro-2-(substitutedphenyl)benzoxazole (**1a-1r**) and 2-(substitutedphenyl)oxazolo[4,5-*b*]pyridine (**2a-2i**) derivatives as novel candidate antitumor agents targeting human DNA topoisomerase enzymes (hTopo I and hTopo II α). Biological activity results were found very promising for the future due to two compounds, 5-nitro-2-(4-butylphenyl)benzoxazole (**1i**) and 2-(4-butylphenyl)oxazolo[4,5-*b*]pyridine (**2i**), that inhibited hTopo II α with 2 μ M IC₅₀ value. These two compounds were also found to be more active than reference drug etoposide. However, **1i** and **2i** did not show any satisfactory cytotoxic activity on the HeLa, WiDR, A549, and MCF7 cancer cell lines. Moreover, molecular docking and molecular dynamic simulations studies for the most active compounds were applied in order to understand the mechanism of inhibition activity of hTopo II α . In addition, *in silico* ADME/Tox studies were performed to predict drug-likeness and pharmacokinetic properties of all the tested compounds.

1. Introduction

Cancer characterized by unregulated proliferation of cells is a major human health problem in the worldwide and the second leading cause of death after cardiovascular disease [1,2]. Hence, on-going researches and discovery of anticancer drugs that have low toxicity and highly potent are still important fields in anti-cancer drug research and development [3]. In drug discovery, “one disease–one target–one drug” approach is more common implementation to reduce unwanted side effects [4]. The development of synthetic topoisomerase inhibitors is an important group of drugs in the treatment of many types of cancer [5].

DNA Topoisomerases (Topo) are enzymes which regulate the conformational or topological changes of DNA by catalyzing the

concerted breakage and reunion of DNA strands during normal cell growth [6]. They solve DNA replication, transcription, recombination, repair, and chromatin assembly in the regulation of DNA topology [7–10]. There are two types of DNA topoisomerases (Type I and Type II) [11,12] based on the number of DNA strands cleaved (one or two, for type I or II, respectively), the nature of the covalent phosphotyrosyl intermediate formed (5' or 3' linkage), and other aspects of enzyme structure and catalysis. Nevertheless, these enzymes all share a common mechanism of transient breakage and reunion of DNA strand(s) [13]. Topo I, changing the DNA topology by breaking the phosphodiester bond between DNA strands is based on the same general mechanism. The phosphoryl group of DNAs is attacked by tyrosyl group of Topo I. This creates a covalent bond between the tyrosyl group and one side of

* Corresponding author.

E-mail address: iyildiz@pharmacy.ankara.edu.tr (I. Yildiz).

¹ These authors (E.K. and E.F.) contributed equally as a first name.

² These authors (G.Y., T.E.B. and S.Y.) contributed equally as a second name.

the broken DNA. At the same time, the free hydroxylated strand is released and rotated. The hydroxyl end of the free strand of DNA attacks the formed phosphotyrosine bond, rebuilds the phosphodiester bond between the two strands and releases the enzyme to the next catalytic cycle [14,15]. Topo II changing the topology of DNA by cleaving both strands of DNA duplex with Mg^{2+} and energy from ATP hydrolysis. Topo II covalently attaches tyrosine to the 5' end of broken DNA, release a free 3' end and allows to passing a second DNA duplex (the transported or T-segment) through a gap (the gate or G-segment) Topo II enzymes can relax both positive and negative supercoils in DNA. [15,16]. Recently, some studies have indicated that Topo II levels increase during cell proliferation and this enzyme appears to be the isoform involved in mitosis [17]. Therefore, inhibition of these enzymes has been considered as targets for the development of novel anticancer agents. Some of the topoisomerase inhibitors such as camptothecin, topotecan irinotecan, etoposide have notable therapeutic efficacy as antitumor drugs [18–23].

All topoisomerase directed agents are able to interfere with at least one step of the catalytic cycle of topoisomerases. Agents able to stabilize the covalent DNA topoisomerase complex (the cleavable complex) are traditionally called Topo II poisons, while agents acting on any of the other steps in the catalytic cycle are called catalytic inhibitors. Catalytic Topo II inhibitors are a heterogeneous group of compounds that might interfere with the binding between DNA and Topo II (aclerubicin and suramin), stabilize noncovalent DNA Topo II complexes (merbarone, ICRF-187, and structurally related bisdioxopiperazine derivatives), or inhibit ATP binding (novobiocin) [24]. Classical Topo II-inhibiting agents such as epipodophylotoxins or anthracyclines interfere with the breakage-reunion reaction of Topo II by stabilizing this cleavable complex. The stabilization of the cleavable complex and not the inhibition of the Topo II activity is supposed to play the decisive role in the cytotoxic effect of the classical Topo II interacting agents [25]. The stabilized cleavable complex leads to both single- and double-strand DNA breaks, which can trigger cellular signal transduction pathways leading to cell death [26]. Accordingly, resistance against classical Topo II-inhibiting agents can result from any process that leads to an altered binding of Topo II to drugs or DNA and a reduced formation of cleavable complexes. Indeed, it was demonstrated that decreased Topo II catalytic activity can mediate drug resistance to cancer cells [27]. Since these drug-resistant tumor cells showed cross resistance to other drugs, this phenotype was designated as altered Topo II multidrug resistance (at-MDR) [28]. The decrease in Topo II activity can be caused by diminished expression levels of both Topo II isoforms [29] as well as by missense mutations within the Topo II isoenzyme encoding genes [30].

Since drug resistance is a major problem in treatment of cancer diseases, it is important to design alternative chemotherapeutic agents.

In 2004, Pinar et al., screened some synthesized 2,5,6-substituted benzoxazole, benzimidazole, benzothiazole and oxazolo[4,5-*b*]pyridine derivatives for their eukaryotic DNA Topo II inhibitory activity in cell free system [31]. Among these compounds, 2-phenoxyethylbenzothiazole ($IC_{50} = 11.4 \mu M$), 2-(2-methoxyphenyl)-6-nitrobenzoxazole ($IC_{50} = 17 \mu M$), 5-methylcarboxylate-2-(phenylthiomethyl)benzimidazole ($IC_{50} = 17 \mu M$), and 6-methyl-2-(2-nitrophenyl)benzoxazole ($IC_{50} = 18.8 \mu M$), were found to be more potent than the clinically used reference drug etoposide ($IC_{50} = 21.8 \mu M$). It was determined that

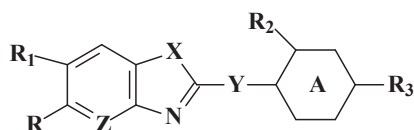
an electron withdrawing substitution in 5 (or 6) position positively affected the activity and in order to demonstrate this, 3D QSAR studies of these compounds (Fig. 1) were performed using CoMFA (Comparative Molecular Field Analysis) and CoMSIA (Comparative Molecular Similarity indices Analysis) methods in 2005 and 2006 [32,33]. With these CoMFA and CoMSIA analysis, the properties of the regions responsible for the activity of the Topo II enzyme have been revealed using potent compounds. These previously published our studies demonstrated that hydrophobic interactions have significant role for enhancing Topo II enzyme inhibitory activity. It was also noticed that hydrophilic substituent on the 5th or 6th position of heterocyclic core was more significant than hydrophobic ones. The other significant knowledge was a hydrophobic group had to have been at the *ortho* and *para* of the phenyl ring of the 2nd position of heterocyclic ring. Moreover, the 3D CoMFA analysis study showed that both an electronegative group at the 5th or 6th position of the heterocyclic structure and an electropositive group on the *ortho* of the phenyl ring in the 2nd position of heterocyclic ring system would increase Topo II enzyme inhibition effect. In addition, both CoMFA and CoMSIA studies indicated that steric properties were found to be important for the activity and activity was reported to be increased by the inclusion of bulky groups at the *ortho* and *para* positions of the phenyl ring in 2nd position of the heterocyclic ring.

Under the light of these studies, in here, an electron-withdrawing and hydrophilic group for 5 (or 6) position and hydrophobic alkyl chains for 2nd position, especially on the *para* of the phenyl ring were selected. Therefore, some of novel 2-(substitutedphenyl)benzoxazole derivatives bearing the nitro group at position 5 (or 6) and 2-(substitutedphenyl)oxazolo[4,5-*b*]pyridines were designed, synthesized in order to determine for their human DNA Topo I and II α inhibitory effects. Their activity was also compared to camptothecine (CPT) (for Topo I) and etoposide (for Topo II), which are well known clinically used drug. Moreover, the most active compounds were analyzed the potential antitumor activity in various cancer lines, as well. *In silico* studies give us some prediction related to how the interaction between ligand and enzyme is and about the ADME/Tox properties. Therefore, in this study we applied molecular docking (Schrödinger) and molecular dynamic (AMBER v14) studies in order to see the interactions between hTopo II α (PID: 5GWK) and the most active compounds. Additionally, ADME/Tox properties of these compounds were predicted by using Accelrys Discovery Studio 3.5 in order to find the “best” drug candidate as hTopo II α inhibitors or antitumor agents.

2. Materials and methods

2.1. Chemical synthesis

All chemicals and solvents were purchased from commercial vendors and used without purification. All reactions were monitored by thin layer chromatography on ready-made silica gel 60 GF₂₅₄ alumina plates (Merck) with visualization of Camag UV light. The melting points were measured with a capillary melting point apparatus (Buchi B540) and were uncorrected. The IR spectra were directly recorded on an Agilent Cary 630 FTIR-Diamond ATR¹ spectrophotometer. The ¹H NMR (Supporting Information) and ¹³C NMR spectra were recorded



Z: CH, N; **X:** O, NH, S; **Y:** -, CH₂, C₂H₄, CH₂O, CH₂S; **A:** Phenyl, Cyclohexyl, Cyclopentyl
R: H, Cl, CH₃, NO₂, NH₂, COOCH₃; **R₁:** H, CH₃, NO₂; **R₂:** F, CH₃, NO₂, OCH₃; **R₃:** H, Cl, CH₃, C₂H₅, C(CH₃)₃, NH₂, NHCH₃, OCH₃, OC₂H₅

Fig. 1. Heterocyclic compounds used in CoMFA and CoMSIA studies [32,33].

employing a VARIAN Mercury 400 High Performance Digital FT-NMR Spectrometer 400 MHz and 100 MHz, respectively. Chemical shifts were reported in ppm (δ) relative to TMS and coupling constants (J) were reported in hertz. Mass spectra were taken on a Waters2965 Alliance Micromass ZQ LC/MS using the ESI method. Elemental analyses were performed by Leco CHNS-932 CHNS-O analyzer. The result of the elemental analyses (C, H, N, S) were within $\pm 0.4\%$ of the calculated amounts.

2.2. General method of synthesis of 2-(substitutedphenyl)benzoxazole (1a-1r) and 2-(substitutedphenyl)oxazolo[4,5-b]pyridine (2a-2i) derivatives

The derivatives were synthesized by heating 0.01 mol appropriate amine with 0.015 mol suitable acid in 24 g polyphosphoric acid (PPA) and stirring for 2–3 h at 120 °C –140 °C. At the end of reaction period, the residue was poured into an ice-water mixture and neutralized with an excess 10% NaOH solution. The residue was boiled with 200 mg charcoal in ethanol and filtered. The crude product was obtained and recrystallized from ethanol. In the present study, all the compounds are original except compounds **1a**, **1c**, **1j**, **1l**, **2a**, **2c-2h** [34–38].

2.2.1. 2-(4-tert-butylphenyl)-5-nitrobenzoxazole (1a)

Yield: 46.80% mp 158–161 °C (Ref. mp: 158 °C) [37]; ESI(+): 297, 48 ($M^+ + H$) (100%); Anal. Calcd. for $C_{17}H_{16}N_2O_3$. 0.1 H_2O C, 68.48; H, 5.47; N, 9.40 Found: C, 68.14; H, 5.72; N, 9.82.

2.2.2. 2-(4-isopropylphenyl)-5-nitrobenzoxazole (1b)

Yield: 43.15%; mp: 149–153 °C; FT-IR (ν_{max}): 3117, 2961, 1556–1617, 1518, 1490, 1343, 1179–1256, 918 cm^{-1} ; 1H NMR (DMSO- d_6 , 400 MHz); δ ppm: 1.24 (d, 6H, $J = 6.8$ Hz, CH_3), 2.95–3.02 (m, 1H, CH), 7.48 (d, 2H, $J = 8.8$ Hz, H-3', H-5'), 7.98 (d, 1H, $J = 9.2$ Hz, H-7), 8.1 (d, 2H, $J = 8.4$ Hz, H-2', H-6'), 8.28 (dd, 1H, $J = 9.2$ Hz, $J = 2.4$ Hz, H-6), 8.57 (d, 1H, $J = 2.4$ Hz, H-4); ^{13}C NMR (DMSO- d_6 , 100 MHz); δ ppm: 23.300, 33.419, 111.488, 115.321, 121.097, 122.971, 127.315, 127.764, 141.877, 141.925, 153.688, 153.833, 165.324; ESI(+): 283, 34 ($M^+ + H$) (100%); Anal. Calcd. for $C_{16}H_{14}N_2O_3$ C, 68.07; H, 5.00; N, 9.92 Found: C, 68.16; H, 4.87; N, 9.88

2.2.3. 2-(4-(trifluoromethyl)phenyl)-5-nitro-benzoxazole (1c)

Yield: 44.09%; mp: 141–146 °C; FT-IR Spektrumu (ν_{max}): 3112, 2908, 1504–1625, 1531, 1435, 1345, 1120, 1064–1112, 691–943 cm^{-1} ; 1H NMR (DMSO- d_6 , 400 MHz); δ ppm: 7.98 (d, 2H, $J = 8.4$ Hz, H-2', H-6'), 8.06 (d, 1H, $J = 9.2$ Hz, H-7), 8.35 (dd, 1H, $J = 8.8$ Hz, $J = 2.4$ Hz, H-6), 8.38 (d, 2H, $J = 8$ Hz, H-3', H-5'), 8.68 (d, 1H, $J = 2.4$ Hz, H-4); ^{13}C NMR (DMSO- d_6 , 100 MHz); δ ppm: 112.044, 116.098, 121.958, 122.323, 125.036, 126.358, 128.511, 129.220, 131.963, 132.283, 141.602, 145.176, 154.016, 163.830; ESI(+): 309.09 ($M^+ + H$) (100%); Anal. Calcd. for $C_{14}H_7F_3N_2O_3$ C, 54.56; H, 2.29; N, 9.09 Found: C, 54.45; H, 2.09; N, 9.25

2.2.4. 2-(3-(methylthio)phenyl)-5-nitrobenzoxazole (1d)

Yield: 40.33%; mp: 130–134 °C; FT-IR (ν_{max}): 3101, 1574–1619, 1522, 1430, 1340, 1079–1267, 788–926 cm^{-1} ; 1H NMR (DMSO- d_6 , 400 MHz); δ ppm: 2.56 (s, 3H, CH_3), 7.52–7.57 (m, 2H, H-2', H-4'), 7.93–7.96 (m, 2H, H-5', H-6'), 8.01 (d, 1H, $J = 8.8$ Hz, H-7), 8.31 (dd, 1H, $J = 9.2$ Hz, $J = 2.4$ Hz, H-6), 8.63 (d, 1H, $J = 2$ Hz, H-4); ^{13}C NMR (DMSO- d_6 , 100 MHz); δ ppm: 14.341, 111.750, 115.666, 121.488, 123.888, 123.911, 126.083, 129.779, 129.870, 140.089, 141.682, 144.996, 153.889, 164.725; ESI(+): 287.29 ($M^+ + H$) (100%); Anal. Calcd. for $C_{14}H_{10}N_2O_3S$ C, 58.74; H, 3.49; N, 9.79; S, 11.19 Found: C, 58.94; H, 3.44; N, 9.92; S, 11.30.

2.2.5. 2-(2,3-dimethylphenyl)-5-nitrobenzoxazole (1e)

Yield: 55.17%; mp: 143–148 °C; FT-IR (ν_{max}): 3106, 1522–1610, 1449, 1345, 1131–1248, 795–875 cm^{-1} ; 1H NMR (DMSO- d_6 , 400 MHz);

δ ppm: 2.36 (s, 3H, CH_3), 2.62 (s, 3H, CH_3), 7.32 (t, 1H, H-4'), 7.45 (d, 1H, $J = 7.6$ Hz, H-7), 7.89 (d, 1H, $J = 7.6$ Hz, H-5'), 8.01 (d, 1H, $J = 8.4$ Hz, H-6'), 8.33 (dd, 1H, $J = 9.2$ Hz, $J = 2.4$ Hz, H-6), 8.65 (d, 1H, $J = 2.4$ Hz, H-4); ^{13}C NMR (DMSO- d_6 , 100 MHz); δ ppm: 16.776, 20.232, 111.557, 115.680, 121.335, 124.932, 125.926, 127.984, 133.415, 137.339, 138.378, 141.834, 153.439, 165.930; ESI(+): 269.36 ($M^+ + H$) (100%); Anal. Calcd. for $C_{15}H_{12}N_2O_3$ C, 67.16; H, 4.51; N, 10.44 Found: C, 67.23; H, 4.59; N, 10.49.

2.2.6. 2-(2,4-dimethylphenyl)-5-nitrobenzoxazole (1f)

Yield: 55.66%; mp: 155–158 °C; FT-IR (ν_{max}): 3108, 1545–1613, 1518, 1433, 1340, 1144–1254, 816–868 cm^{-1} ; 1H NMR (DMSO- d_6 , 400 MHz); δ ppm: 2.35 (s, 3H, CH_3), 2.71 (s, 3H, CH_3), 7.26 (t, 2H, H-3', H-5'), 8.00 (d, 1H, $J = 9.2$ Hz, H-7), 8.04 (d, 1H, $J = 8.4$ Hz, H-6'), 8.31 (dd, 1H, $J = 8.6$ Hz, $J = 2.4$ Hz, H-6), 8.63 (s, 1H, H-4); ^{13}C NMR (DMSO- d_6 , 100 MHz); δ ppm: 20.861, 21.600, 107.205, 119.725, 120.525, 121.592, 127.147, 129.936, 132.618, 138.928, 142.585, 144.529, 146.85, 148.773, 167.099; ESI(+): 269.28 ($M^+ + H$) (100%); Anal. Calcd. for $C_{15}H_{12}N_2O_3$ C, 67.16; H, 4.51; N, 10.44 Found: C, 66.82; H, 4.60; N, 10.34.

2.2.7. 2-(2,5-dimethylphenyl)-5-nitrobenzoxazole (1g)

Yield: 45.58%; mp: 135–143 °C; FT-IR (ν_{max}): 3106, 2924, 1602–1617, 1522, 1435, 1334, 1176–1256, 987–703 cm^{-1} ; 1H NMR (DMSO- d_6 , 400 MHz); δ ppm: 2.34 (s, 3H, CH_3), 2.66 (s, 3H, CH_3), 7.31 (s, 2H, H-3', H-4'), 7.90 (s, 1H, H-6'), 7.97 (d, 1H, $J = 8.8$ Hz, H-7), 8.28 (dd, 1H, $J = 8.8$, $J = 2$ Hz, H-6), 8.58 (d, 1H, $J = 2$ Hz, H-4); ^{13}C NMR (DMSO- d_6 , 100 MHz); δ ppm: 20.312, 21.311, 111.503, 115.587, 121.318, 124.084, 129.997, 131.971, 132.801, 135.666, 135.849, 141.778, 144.841, 153.322, 165.007; ESI(+): 269.33 ($M^+ + H$) (100%); Anal. Calcd. for $C_{15}H_{12}N_2O_3$ C, 67.16; H, 4.51; N, 10.44 Found: C, 66.87; H, 4.72; N, 10.34.

2.2.8. 2-(3,5-dimethylphenyl)-5-nitrobenzoxazole (1h)

Yield: 53.87%; mp: 172–178 °C; FT-IR (ν_{max}): 3104, 2916, 1604–1621, 1518, 1435, 1345, 1058–1231, 691–926 cm^{-1} ; 1H NMR (DMSO- d_6 , 400 MHz); δ ppm: 2.36 (s, 3H, CH_3), 7.29 (s, 1H, H-4'), 7.79 (s, 2H, H-2', H-6'), 7.98 (d, 1H, $J = 9.2$ Hz, H-7), 8.29 (dd, 1H, $J = 8.8$ Hz, $J = 2.4$ Hz, H-6), 8.58 (d, 1H, $J = 2$ Hz, H-4); ^{13}C NMR (DMSO- d_6 , 100 MHz); δ ppm: 20.747, 111.686, 115.564, 121.401, 125.364, 134.348, 138.852, 141.900, 145.032, 153.955, 165.530; ESI(+): 269.30 ($M^+ + H$) (100%); Anal. Calcd. for $C_{15}H_{12}N_2O_3$ C, 67.16; H, 4.51; N, 10.44 Found: C, 67.02; H, 4.15; N, 10.54.

2.2.9. 2-(4-butylphenyl)-5-nitrobenzoxazole (1i)

Yield: 45.24%; mp: 108–113 °C; FT-IR (ν_{max}): 3071, 2955, 1608–1522, 1340, 1235–1060, 920–732 cm^{-1} ; 1H NMR (DMSO- d_6 , 400 MHz); δ ppm: 0.92 (t, 3H, CH_3), 1.29–1.38 (m, 2H, CH_2), 1.56–1.64 (m, 2H, CH_2), 2.67 (t, 2H, CH_2), 7.43 (d, 2H, $J = 8$ Hz, H-3', H-5'), 7.98 (d, 1H, $J = 8.8$ Hz, H-7), 8.08 (d, 2H, $J = 8.8$ Hz, H-2', H-6'), 8.29 (dd, 1H, $J = 9.2$ Hz, $J = 2.4$ Hz, H-6), 8.58 (d, 1H, $J = 2.4$ Hz, H-4); ^{13}C NMR (DMSO- d_6 , 100 MHz); δ ppm: 13.652, 21.669, 32.581, 34.745, 111.556, 115.389, 121.180, 122.864, 127.696, 129.296, 141.922, 144.948, 147.904, 153.860, 165.408; ESI(+): 297.4 ($M^+ + H$) (100%); Anal. Calcd. for $C_{17}H_{16}N_2O_3$ C, 68.91; H, 5.44; N, 9.45 Found: C, 69.19; H, 5.75; N, 9.47.

2.2.10. 2-(4-tert-butylphenyl)-6-nitrobenzoxazole (1j)

Yield: 44.15%; mp 164–166 °C (Ref. mp: 160–165 °C) [34]; ESI(+): 297.40 ($M^+ + H$) (100%); Anal. Calcd. for $C_{17}H_{16}N_2O_3$ C, 68.91; H, 5.44; N, 9.45 Found: C, 69.11; H, 5.67; N, 9.38

2.2.11. 2-(4-isopropylphenyl)-6-nitrobenzoxazole (1k)

Yield: 39.40%; mp: 112–123 °C; FT-IR (ν_{max}): 3110, 2963, 1554–1606, 1543, 1464, 1341, 1060–1170, 922 cm^{-1} ; 1H NMR (DMSO- d_6 , 400 MHz); δ ppm: 1.26 (d, 6H, $J = 6.8$ Hz, CH_3), 3.01 (m, 1H,

CH), 7.52 (d, 2H, $J = 8$ Hz, H-3', H-5'), 7.98 (d, 1H, $J = 8,8$ Hz, H-4), 8.14 (d, 2H, $J = 8$ Hz, H-2', H-6'), 8.29 (dd, 1H, $J = 9,2$ Hz, $J = 2,4$ Hz, H-5), 8.68 (d, 1H, H-7); ^{13}C NMR (DMSO- d_6 , 100 MHz); δ ppm: 23.348, 33.506, 107.391, 119.697, 120.772, 122.997, 127.417, 127.996, 144.516, 146.955, 149.386, 154.034, 166.805; ESI(+): 283.32 (M^+ +H) (100%); Anal. Calcd. for $\text{C}_{16}\text{H}_{14}\text{N}_2\text{O}_3 \cdot 0.4 \text{H}_2\text{O}$ C, 66.38; H, 5.15; N, 9.67 Found: C, 66.72; H, 5.05; N, 9.73.

2.2.12. 2-(4-(trifluoromethyl)phenyl)-6-nitro-benzoxazole (1l)

Yield: 44.46%; mp: 129–133 °C; FT-IR (ν_{max}): 3121, 1556–1619, 1524, 1426, 1343, 1259, 1131, 1067–1259, 756–818 cm^{-1} ; ^1H NMR (DMSO- d_6 , 400 MHz); δ ppm: 8.00 (d, 3H, $J = 8,4$ Hz, H-2', H-6'), 8.06 (d, 1H, $J = 8,4$ Hz, H-4), 8.32 (dd, 1H, $J = 8,8$ Hz, $J = 2,4$ Hz, H-5), 8.41 (d, 2H, $J = 8$ Hz, H-3', H-5'), 8.76 (d, 1H, $J = 2$ Hz, H-7); ^{13}C NMR (DMSO- d_6 , 100 MHz); δ ppm: 107.928, 120.482, 121.059, 122.329, 125.041, 126.445, 128.721, 129.286, 132.145, 132.466, 145.194, 146.540, 149.701, 165.250; ESI(+): 309.45 (M^+ +H) (100%); Anal. Calcd. for $\text{C}_{14}\text{H}_7\text{F}_3\text{N}_2\text{O}_3$ C, 54.56; H, 2.29; N, 9.09 Found: C, 54.37; H, 2.17; N, 9.20

2.2.13. 2-(2,3-dimethylphenyl)-6-nitrobenzoxazole (1m)

Yield: 50.86%; mp: 143–149 °C; FT-IR (ν_{max}): 3108, 1589–1610, 1518, 1435, 1345, 1058, 726–825 cm^{-1} ; ^1H NMR (DMSO- d_6 , 400 MHz); δ ppm: 2.34 (s, 3H, CH_3), 2.61 (s, 3H, CH_3), 7.31 (d, 1H, $J = 7,6$ Hz, H-4'), 7.44 (d, 1H, $J = 6,4$ Hz, H-4), 7.89 (d, 1H, $J = 6,8$ Hz, H-5'), 8.,00 (d, 1H, $J = 8,4$ Hz, H-6'), 8.27 (d, 1H, $J = 7,6$ Hz, H-5), 8.66 (s, 1H, H-7); ^{13}C NMR (DMSO- d_6 , 100 MHz); δ ppm: 16.748, 20.153, 107.380, 119.966, 120.556, 124.993, 125.923, 128.116, 133.592, 137.452, 138.401, 144.723, 146.704, 148.967, 167.478; ESI(+): 269.34 (M^+ +H) (100%); Anal. Calcd. for $\text{C}_{15}\text{H}_{12}\text{N}_2\text{O}_3$ C, 67.16; H, 4.51; N, 10.44 Found: C, 66.77; H, 4.10; N, 10.63.

2.2.14. 2-(2,4-dimethylphenyl)-6-nitrobenzoxazole (1n)

Yield: 40%; mp: 164–170 °C; FT-IR (ν_{max}): 3106, 2957, 1540–1606, 1518, 1433, 1340, 1121–1144, 816–868 cm^{-1} ; ^1H NMR (DMSO- d_6 , 400 MHz); δ ppm: 2.35 (s, 3H, CH_3), 2.71 (s, 3H, CH_3), 7.26 (t, 2H, H-3', H-5'), 7.97 (d, 1H, $J = 8,4$ Hz, H-4), 8.04 (d, 1H, $J = 8,4$ Hz, H-6'), 8.27 (dd, 1H, $J = 8,8$ Hz, $J = 2,4$ Hz, H-5), 8.64 (d, 1H, $J = 2$ Hz, H-7); ^{13}C NMR (DMSO- d_6 , 100 MHz); δ ppm: 20.861, 21.600, 107.205, 119.725, 120.525, 121.592, 127.147, 129.936, 132.618, 138.928, 142.585, 144.529, 146.853, 148.773, 167.099; ESI(+): 297.48 (M^+ +H) (100%); Anal. Calcd. for $\text{C}_{15}\text{H}_{12}\text{N}_2\text{O}_3$ C, 67.16; H, 4.51; N, 10.44 Found: C, 66.97; H, 4.47; N, 10.37.

2.2.15. 2-(2,5-dimethylphenyl)-6-nitrobenzoxazole (1o)

Yield: 40.14%; mp: 133–135 °C; FT-IR (ν_{max}): 3108, 2920, 1539–1620, 1513, 1435, 1349, 1062, 689–930 cm^{-1} ; ^1H NMR (DMSO- d_6 , 400 MHz); δ ppm: 2.36 (s, 3H, CH_3), 2.68 (s, 3H, CH_3), 7.33 (t, 2H, H-3', H-4'), 7.94 (s, 1H, H-6'), 7.99 (d, 1H, $J = 9,2$ Hz, H-4), 8.27 (dd, 1H, $J = 9,2$ Hz, $J = 2,4$ Hz, H-5), 8.66 (d, 1H, $J = 2,4$ Hz, H-7); ^{13}C NMR (DMSO- d_6 , 100 MHz); δ ppm: 20.277, 21.314, 107.322, 119.888, 120.589, 124.071, 130.122, 132.004, 133.010, 135.662, 136.020, 144.608, 146.749, 148.814, 166.996; ESI(+): 269.35 (M^+ +H) (100%); Anal. Calcd. for $\text{C}_{15}\text{H}_{12}\text{N}_2\text{O}_3$ C, 67.16; H, 4.51; N, 10.44 Found: C, 67.54; H, 4.57; N, 10.45.

2.2.16. 2-(3,5-dimethylphenyl)-6-nitrobenzoxazole (1p)

Yield: 42.68%; mp: 161–169 °C; FT-IR (ν_{max}): 3099, 2918, 1545–1600, 1507, 1464, 1343, 1056–1265, 684–829 cm^{-1} ; ^1H NMR (DMSO- d_6 , 400 MHz); δ ppm: 2.38 (s, 6H, CH_3), 7.3 (s, 1H, H-4'), 7.79 (s, 2H, H-2', H-6'), 7.94 (d, 1H, $J = 8,4$ Hz, H-4), 8.27 (dd, 1H, $J = 8,6$ Hz, $J = 2$ Hz, H-5), 8.61 (d, 1H, $J = 2$ Hz, H-7); ^{13}C NMR (DMSO- d_6 , 100 MHz); δ ppm: 20.556, 107.213, 119.664, 120.647, 125.120, 125.341, 134.356, 138.653, 144.529, 146.761, 149.276, 166.795; ESI(+): 269.21 (M^+ +H) (100%); Anal. Calcd. for $\text{C}_{15}\text{H}_{12}\text{N}_2\text{O}_3$ C, 67.16; H, 4.51; N, 10.44 Found: C, 66.91; H, 4.28; N, 10.48.

2.2.17. 2-(4-butylphenyl)-6-nitrobenzoxazole (1r)

Yield: 28%; mp: 84–86 °C; FT-IR (ν_{max}): 3106, 2933, 1614–1517, 1340, 1269–1125, 881–732 cm^{-1} ; ^1H NMR (DMSO- d_6 , 400 MHz); δ ppm: 0.91 (t, 3H, CH_3), 1.28–1.37 (m, 2H, CH_2), 1.55–1.62 (m, 2H, CH_2), 2.66 (t, 2H, CH_2), 7.41 (d, 2H, $J = 8,4$ Hz, H-3', H-5'), 7.94 (d, 1H, $J = 8,8$ Hz, H-4), 8.07 (d, 2H, $J = 8$ Hz, H-2', H-6'), 8.26 (dd, 1H, $J = 8$ Hz, $J = 2,4$ Hz, H-5), 8.62 (d, 1H, $J = 2,4$ Hz, H-7); ^{13}C NMR (DMSO- d_6 , 100 MHz); δ ppm: 13.706, 21.768, 32.604, 34.821, 107.350, 119.695, 120.77, 122.788, 127.840, 129.288, 144.460, 146.959, 148.194, 149.337, 166.818; ESI(+): 297.3 (M^+ +H) (100%); Anal. Calcd. for $\text{C}_{17}\text{H}_{16}\text{N}_2\text{O}_3$ C, 68.91; H, 5.44; N, 9.45 Found: C, 68.92; H, 5.58; N, 9.45.

2.2.18. 2-(4-tert-butylphenyl)oxazolo[4,5-b]pyridine (2a)

Yield: 43.39%; mp 140–144 °C (Ref. mp: 142 °C) [36]; ESI(+): 253.18 (M^+ +H) (100%); Anal. Calcd. for $\text{C}_{16}\text{H}_{16}\text{N}_2\text{O}$ C, 76.16; H, 6.39; N, 11.10 Found: C, 76.67; H, 6.64; N, 11.06.

2.2.19. 2-(4-isopropylphenyl)oxazolo[4,5-b]pyridine (2b)

Yield: 43.1%; mp: 101–103 °C; FT-IR (ν_{max}): 3065, 2957, 1615, 1548, 1496, 1261–1179, 934–918 cm^{-1} ; ^1H NMR (DMSO- d_6 , 400 MHz); δ ppm: 1.26 (d, 6H, $J = 6,4$ Hz, CH_3), 3.34 (s, 1H, CH), 7.46 (m, 1H, H-6), 7.52 (d, 2H, $J = 8$ Hz, H-3', H-5'), 8.18 (d, 2H, $J = 8$ Hz, H-2', H-6'), 8.23 (dd, 1H, $J = 8$ Hz, $J = 1,6$ Hz, H-7), 8.55 (dd, 1H, $J = 4,8$ Hz, $J = 1,6$ Hz, H-5); ^{13}C NMR (DMSO- d_6 , 100 MHz); δ ppm: 23.414, 33.503, 118.856, 120.525, 123.497, 127.353, 127.772, 142.624, 146.396, 153.619, 155.578, 164.897; ESI(+): 239.04 (M^+ +H) (100%); Anal. Calcd. for $\text{C}_{15}\text{H}_{14}\text{N}_2\text{O}$ C, 75.61; H, 5.92; N, 11.76 Found: C, 75.38; H, 6.10; N, 11.63.

2.2.20. 2-(4-(trifluoromethyl)phenyl)oxazolo[4,5-b]pyridine (2c)

Yield: 40.32%; mp 163–165 °C (Ref. mp: 162–164 °C) [38]; ESI(+): 265.12 (M^+ +H) (100%); Anal. Calcd. for $\text{C}_{13}\text{H}_7\text{F}_3\text{N}_2\text{O}$. 0.05 H_2O C, 58.89; H, 2.69; N, 10.56 Found: C, 58.67; H, 2.66; N, 10.58.

2.2.21. 2-(3-(methylthio)phenyl)oxazolo[4,5-b]pyridine (2d)

Yield: 42.99% mp 83–85 °C (Ref. mp: 82–84 °C) [35]; ESI(+): 243.3 (M^+ +H) (100%); Anal. Calcd. for $\text{C}_{13}\text{H}_{10}\text{N}_2\text{OS}$. 0.1 H_2O C, 63.96; H, 4.21; N, 11.47; S, 13.13 Found: C, 63.92; H, 4.35; N, 11.30; S, 13.10.

2.2.22. 2-(2,3-dimethylphenyl)oxazolo[4,5-b]pyridine (2e)

Yield: 57.14%; mp 72–74 °C (Ref. mp: 72–73 °C) [35]; ESI(+): 225.38 (M^+ +H) (100%); Anal. Calcd. for $\text{C}_{14}\text{H}_{12}\text{N}_2\text{O}$ C, 74.98; H, 5.39; N, 12.49 Found: C, 75.13; H, 5.52; N, 12.35.

2.2.23. 2-(2,4-dimethylphenyl)oxazolo[4,5-b]pyridine (2f)

Yield: 47.74%; mp: 94–96 °C (Ref. mp: 93–95 °C) [35]; ESI(+): 225.06 (M^+ +H) (100%); Anal. Calcd. for $\text{C}_{14}\text{H}_{12}\text{N}_2\text{O}$ C, 74.98; H, 5.39; N, 12.49 Found: C, 75.25; H, 5.53; N, 12.40.

2.2.24. 2-(3,5-dimethylphenyl)oxazolo[4,5-b]pyridine (2g)

Yield: 53.69%; mp 157–159 °C (Ref. mp: 155–157 °C) [35]; ESI(+): 225.25 (M^+ +H) (100%); Anal. Calcd. for $\text{C}_{14}\text{H}_{12}\text{N}_2\text{O}$. 0.6 H_2O C, 71.53; H, 5.66; N, 11.91 Found: C, 71.29; H, 5.31; N, 11.75.

2.2.25. 2-(2,5-dimethylphenyl)oxazolo[4,5-b]pyridine (2h)

Yield: 44.57%, mp 87–89 °C (Ref. mp: 86–87 °C) [35]; ESI(+): 225.07 (M^+ +H) (100%); Anal. Calcd. for $\text{C}_{14}\text{H}_{12}\text{N}_2\text{O}$ C, 74.98; H, 5.39; N, 12.49 Found: C, 75.18; H, 5.54; N, 12.38.

2.2.26. 2-(4-butylphenyl)oxazolo[4,5-b]pyridine (2i)

Yield: 47.38%; mp: 76–79 °C; FT-IR (ν_{max}): 3060, 2953, 1578, 1466, 1049–1265, 795–930 cm^{-1} ; ^1H NMR (DMSO- d_6 , 400 MHz); δ ppm: 0.916 (t, 3H, CH_3), 1.31–1.38 (m, 2H, CH_2), 1.57–1.65 (m, 2H, CH_2), 2.69 (t, 2H, CH_2), 7.44–7.48 (m, 3H, H-6, H-3', H-5'), 8.16 (d, 2H, $J = 8,4$ Hz, H-2', H-6'), 8.23 (dd, 1H, $J = 8$ Hz, $J = 1,6$ Hz, H-7), 8.54 (dd, 1H, $J = 5$ Hz, $J = 1,2$ Hz, H-5); ^{13}C NMR (DMSO- d_6 , 100 MHz); δ ppm:

13.691, 21.699, 32.649, 34.776, 118.872, 120.548, 123.352, 127.665, 129.296, 142.639, 146.403, 147.798, 155.593, 164.951; ESI(+): 253.20 (M⁺+H) (100%); Anal. Calcd. for C₁₆H₁₆N₂O. 0,6 H₂O C, 73.03; H, 6.53; N, 10.64 Found: C, 72.89; H, 6.41; N, 10.59.

2.3. Biological activity studies

2.3.1. Topoisomerase I and II α enzyme inhibition

Human DNA topoisomerase I and II α (hTopo I and hTopo II α) inhibitory activities of the tested compounds were determined by plasmid relaxation assay which could measure the conversion of supercoiled pBR322 plasmid DNA to its relaxed form [39,40]. In all experiments, the final concentration of DMSO was 1% and control samples contained an equivalent amount of vehicle. Recombinant purified human Topo I and II α were purchased from TopoGEN (PortOrange, FL, USA). All other common laboratory chemicals were of the highest grade available.

Firstly, hTopo I and II α enzymes inhibition of derivatives were screened at the concentration of 3 mM, and dose-dependent experiments were carried out with various concentrations (0.5–3 mM for hTopo I and 8–1000 μ M for hTopo II α) of the most effective compounds that significantly inhibited the enzymes. Finally, optical intensity of each concentration of the compounds was compared with the control to calculate inhibition percentages. With these percentages, IC₅₀ (50% inhibition concentrations) values of the compounds were calculated using the S-probit analysis program.

For hTopo I relaxation assay, reaction mixture included 0.2 μ g of supercoiled pBR322 plasmid DNA, 1 U of hTopo I and enzyme buffer (10 mM Tris-HCl (pH 7.5), 100 mM NaCl, 1 mM PMSF, 1 mM β -mercaptoethanol). Six different concentrations (0.5–3 mM) of the compounds were added reaction mixture without plasmid, the enzyme and test compounds were preincubated for 5 min at 37 °C. Enzyme reactions were started by addition of DNA and incubated 30 min at 37 °C. The reactions were terminated by stop solution containing 1% SDS and 6X loading buffer.

For hTopo II α relaxation assay, the reaction mixture had a total volume of 10 μ L containing 10 mM TrisHCl (pH 7.9), 50 mM NaCl, 50 mM KCl, 5 mM MgCl₂, 0.1 mM EDTA, 15 mL/mL bovine serum albumin (BSA), 1 mM ATP, 0.3 mM pBR322 plasmid DNA, 1 U of human DNA Topo II α enzyme and different concentrations of compounds. The mixture was incubated for 1 h at 37 °C. After incubation period, 3 mL of loading buffer in electrophoresis buffer TAE (60 mM Tris, 30 mM acetic acid and 1.5 mM EDTA, pH 8.0) was added.

After hTopo I and hTopo II α enzyme and derivatives were incubated and reactions were terminated, the samples were electrophoresed in a horizontal 1% agarose gel in TAE buffer (40 mM Tris acetate, 2 mM EDTA, pH 8.0) at 45 V for 3 h at room temperature. The gels were stained with ethidium bromide (1 μ g/ml) and photographed under UV illumination. Band distributions were analysed by a GDS 8000 Complete Gel Documentation and Analysis System (Gel Works 1D Intermediate, version 2.5; UltraViolet Products).

Standard drugs, camptothecin (CPT) for hTopo I and etoposide for hTopo II α , were used as positive controls. All experiments were repeated for a minimum of two times.

2.3.1.1. Analysis of data for relaxation assays. Topoisomerase enzyme activities were measured by the optical rate of different forms of DNA bands on agarose gel electrophoresis. Inhibition percentages were calculated by bands of intensity difference between control and compound applied wells. We analyzed supercoiled-relaxed DNA bands for catalytic inhibition. We assumed supercoiled DNA without enzyme well as a one hundred percent of enzyme was inhibited. We used direct proportion to calculate inhibition percentages of the remaining supercoiled DNA intensity that belonged to tested compounds in each well. If inhibition was not obtained at any concentration of a tested compound it

was assumed to have no inhibitory activity (NE) on human DNA Topo I and II α .

2.3.2. In vitro anticancer activities

The cytotoxicity of test compounds was assessed using a cell death assay based on detection of cells by sulforhodamine-B (SRB) according to procedure of Vichai and Kitikira [41,42].

In this study, four different human cancer cell lines [HeLa (human epithelial adenocarcinoma cell line of the cervix), Widr (human colorectal adenocarcinoma cell line of the colon), A549 (human epithelial carcinoma cell line of the lung), MCF7 (human epithelial adenocarcinoma cell line of the breast)] were used. All cell lines were cultured in DMEM (Dulbecco's Modified Eagle Medium) supplemented with 10% FBS, 45 IU/ml penicillin and 45 IU/ml streptomycin at 37 °C in a humidified atmosphere of 5% CO₂. The cells were inoculated into 96-well micro titer plates at a density of 1×10^4 cells per well. After cell inoculation, the micro titer plates were incubated for 24 h to attached cells on well surface. Test compounds prepared in DMSO were dissolved in cell culture medium at appropriate final concentrations and added each well. After the addition of compounds, plates were incubated for 48 h at 37 °C and 5% CO₂. Cells were fixed by the gentle addition of 50 mL of cold 10% (w/v) and incubated for 60 min at 4 °C. After incubation were plates washed with tap water for four times and SRB solution at 0.4% (w/v) in 1% acetic acid has been added to each well and the plates were incubated for 30 min at room temperature. Then the plates were rinsed quickly four times with 1% acetic acid to removed unbound excess dye. Bound stain was subsequently eluted with 10 mM tris base solution (pH 10.5) and the absorbance was read on an Elisa plate reader at 510 nm. Percentage growth for each concentrations of compound was calculated on a plate-by-plate basis for test wells relative to control wells. Analyses of cell growth percentage were performed using GraphPad Prism (GraphPad Software Inc and calculated 50% cell growth inhibition (IC₅₀) value of each test compounds.

All experiments were repeated for a minimum of two times with each experiment done in three replicates. Camptothecin and Etoposide were used as the positive control drugs.

2.4. Molecular docking studies

Molecular docking studies were performed by using Schrödinger molecular modeling software (Schrödinger Release 2018-2, LLC, New York, NY, USA) [43,44]. Ligands were prepared by using LigPrep module, the 2D structures of the ligands converted to the full 3D structure by assigning the OPLS-2005 force field. LigPrep can generate the expected ionized forms at significant concentrations corresponding to the pH 7.0 ± 3.0 ; generate variations, verification and optimize the structures. It generates maximum 32 stereochemical structures per ligand. Binding of ligands to the receptors adopts more than one conformation and the lowest energy conformer is important for docking studies. Crystal structure of human Topo II α enzyme complexed with known inhibitor; etoposide was extracted from the Protein Data Bank (PDB ID: 5GWK) (Fig. 3a). Prior to docking the ligands onto the protein's active site, the protein was prepared using protein preparation wizard of Schrödinger software. During the protein preparation all hetero atoms and water molecules were removed. Hydrogen atoms were added, and the active site of the protein was defined for generating the grid. The grid box was limited to the size of 20 Å at the active site. Finally docking studies were carried out using GLIDE (Grid-based Ligand Docking with Energetics) module of Schrödinger Software, the ligands were docked into the prepared grid by using "Extra precision mode" and no constraints were defined. The docking method was first validated by docking of the known inhibitor, etoposide with 0.42 Å RMSD (root-mean-square deviation) value. To determine the spatial fit into the active site of receptor, favorable ligand poses were generated, and best fitted conformations of the ligands were evaluated and minimized for generating glide scores. To predict the binding affinities and best

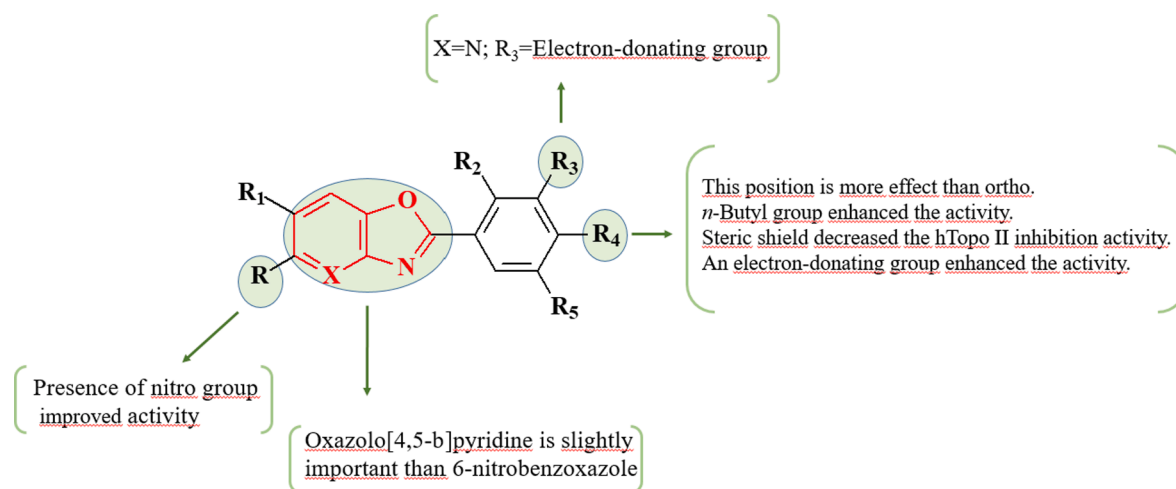


Fig. 2. Structure-hTopo II α inhibition activity relationship of the synthesized compounds.

alignment of the compounds at the active site of the enzyme, hydrogen bonds and π interactions formed with the surrounding amino acids and glide scores were used. All the results were presented in Table 3.

2.5. Molecular dynamic simulations methods

2.5.1. Structural models

The atomic coordinates of DNA Topo II α from human have been deposited in the Protein Data Bank (www.rcsb.org; PDB accession no. 5GWK) [45] (Fig. 3a). hTopo II α was co-crystallized with a part of DNA helix and an inhibitor of receptor, etoposide.

Receptor crystallized in dimer form. Subunit A was chosen was used for docking protocol. All the other heteroatoms except the interested part of DNA helix (i.e., nonreceptor atoms such as redundant water molecules, ions, co-crystallized ligand, etc.) were also removed. For the preparation of receptor Gasteiger charges and polar hydrogens were assigned, and the receptor input file was prepared in PDBQT format for AutoDock Vina by using the Auto-Dock Tools package [46]. Ligands were drawn with Discovery Studio Client 3.5 [47]. The conformations were fixed with the “clean geometry” option of this package. Clean Geometry tool uses a fast, DREIDING-like force field to optimize the structure geometry. The tool improves the geometry of the molecule and results in an approximate 3D structure. For all ligands, including O95, the nonpolar hydrogen atoms were merged, and the Gasteiger charges were assigned. Later, ligand input files were also arranged in PDBQT format using the AutoDock Tools package. The binding sphere was selected around the inhibitor EVP using the binding site tools.

2.5.2. Small molecule docking

Compounds were docked into the binding site of D2R by Auto-dock_vina v1.5.6. The docking area was determined in the crystal structure, by a grid box of 60 Å 50 Å 40 Å using a 0.375 Å grid point spacing in AutoGrid. The docking grid box was defined with the x, y, and z centers as 18.464, -40.422, and -61.005, respectively. Auto-Dock Vina uses a global heuristic optimizer algorithm, Iterated Local Search, with a local optimization algorithm called Broyed-Fletcher-Goldfarb-Shanno (BFGS) [46]. The docking conformations of ligands in the binding sites of the receptor were searched with this Iterated Local Search Global Optimizer algorithm with a Monte Carlo sampling technique as a molecular mechanic method. Semiflexible algorithm was used in docking protocol. Docked coordinates were visualized and selected by MGLtools v1.5.6 [48].

2.5.3. Simulation procedure

Protonation, ion addition and solvation of the initial structure of the

complex species as well as its parameterization was implemented by AMBER14SB force field available in the LEAP module of AMBER v14 [49] suite of programs. The complex molecule was solvated in LEAP by putting together small units of TIP3 water boxes in dimensions of 18.774 Å \times 18.774 Å \times 18.774 Å to constitute a rectangular water box. Solvent unit box means; size of the box of 216 water molecules (WAT-BOX216) that will be used to overlay the solute, remove water molecules that are too close to or inside the solute, and be trimmed to the desired size. The distance between the outer boundary of the octahedral solvent box and the solute surface was set to 10 Å. A space of 0.4 Å was used to set water molecules at the solute-solvent boundary.

Relaxation and temperature equilibration of the solvated complex structure were implemented by the PMEMD module of AMBER v14, and molecular dynamics (MD) computations were carried out by the PMEMD.CUDA module of AMBER v.14, running at the TR-Grid e-Infrastructure of Turkey. The protein-DNA helix-ligand systems were preheated up to 298.15 K over 100 ps (50000 iterations and 2 fs for each of them), during which the protein and the ligand were strongly restrained. Finally, at least 75 nsec of production MD runs were implemented with no restrains for the complex systems at 1 bar and 298.15 K, which utilized the Langevin dynamics algorithm (with a collision frequency of 1 ps⁻¹ and a velocity limit of 10 Kelvin) for keeping the temperature constant and SHAKE algorithm. Structural changes in MD results of enzyme-DNA complex system had visualized and analyzed by Chimera v1.14 [50] molecular modeling program (Figs. 7–10).

2.6. In silico ADME/Tox studies

2.6.1. Molecular property analysis

Chemical structures of compounds were prepared in mol file using ChemDraw 12.0 and molecular properties were calculated using Accelrys Discovery Studio 3.5. All the ligands were screened for Lipinski's Rule of 5 [51] and Veber rules [52]. All of the data was presented in Table 4.

2.6.2. ADME/Tox prediction

ADME/Tox (ADMET) protocol in Discovery studio 3.5 [47] were used for deploying ADMET properties of all synthesized molecules (1a-1r, 2a-2i). This model calculates some pharmacokinetic properties like aqueous solubility, blood brain barrier penetration (BBB), cytochrome P450 (CYP450) 2D6 inhibition, hepatotoxicity, plasma protein binding and human intestinal absorption (HIA) from compounds structure and also predicts some toxicity properties such as AMES and developmental toxicity potential (DTP).

Aqueous solubility calculations use base 10 logarithm of the molar

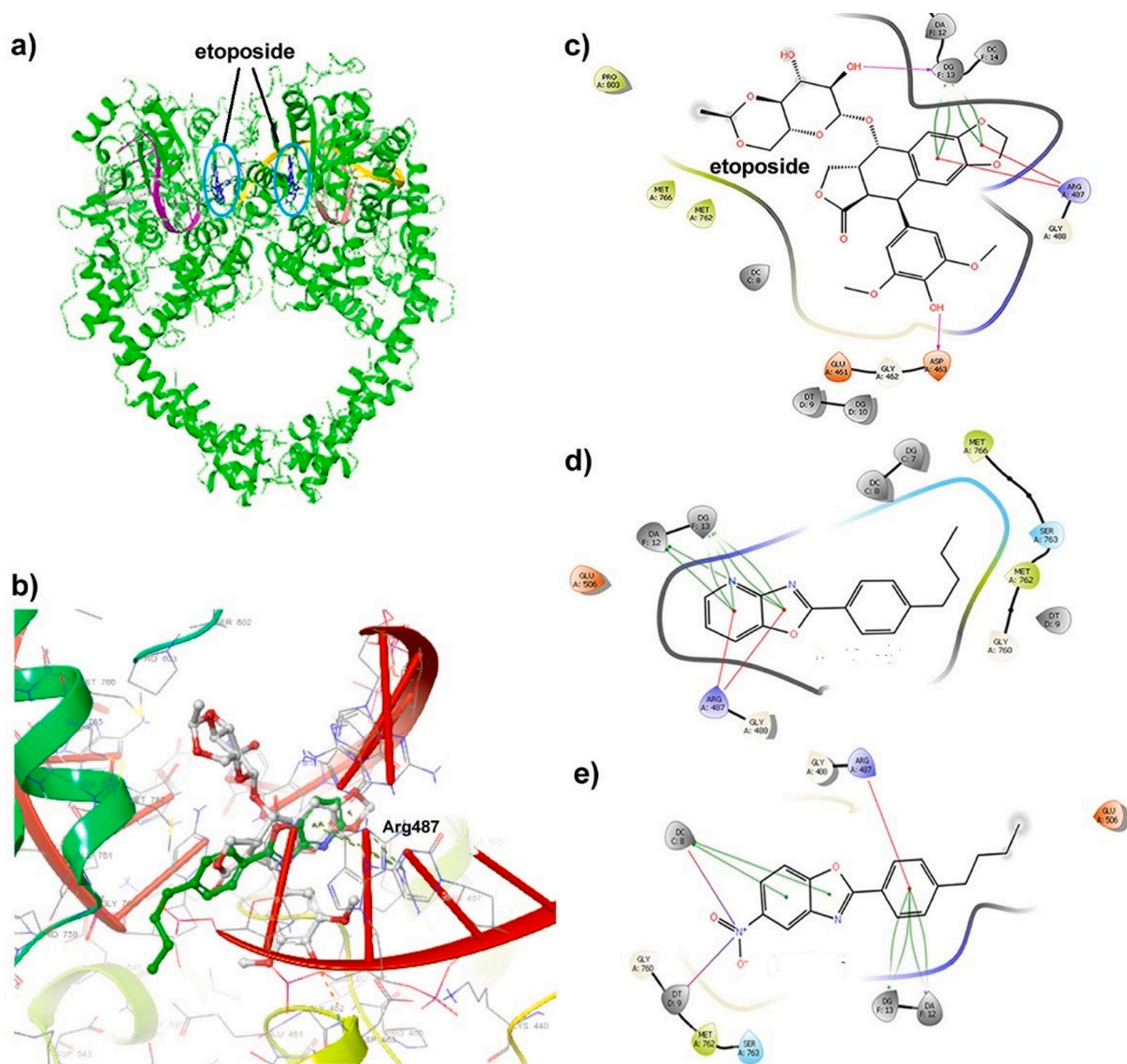


Fig. 3. (a) Crystal structure of hTopo II α enzyme complexed with etoposide (PDB ID: 5GWK). (b) Superposition of 2i and etoposide: both have *pi* interactions with Arg487. (c) Docked position of etoposide: compound revealed H-bond with deoxyguanosin DG13, and Asp463; *pi-pi* stacking with deoxyguanosin DG13; *pi*-cation interactions with Arg487. (d) Docked position of 2i: compound revealed *pi-pi* stacking with deoxyadenosine DA12 and deoxyguanosin DG13, *pi*-cation interaction with Arg487. (e) Docked position of 1i: compound revealed *pi-pi* stacking with deoxycytidine DC8, deoxyadenosine DA12 and deoxyguanosin DG13, *pi*-cation interaction with Arg487.

solubility as predicted by linear regression to predict the solubility of each compound in water at 25 °C [53].

BBB model predicts the blood brain barrier penetration of a molecule after oral administration by using quantitative linear regression model, as well as 95% and 99% confidence ellipses in the PSA_{2D} and AlogP₉₈ plane [54].

The cytochrome P450 2D6 (CYP2D6) model predicts CYP2D6 enzyme inhibition using 2D chemical structure as input. The classification whether a compound is an CYP2D6 inhibitor using the cutoff Bayesian score of 0.162 (obtained by minimizing the total number of false positives and false negatives) [55].

The hepatotoxicity model predicts potential organ toxicity for a wide range of structurally diverse compounds. The classification whether a compound is hepatotoxic using the cutoff Bayesian score of -0.4095 (obtained by minimizing the total number of false positives and false negatives) [56].

The plasma protein binding model predicts whether a compound is likely to be highly bound ($\geq 90\%$ bound) to carrier proteins in the blood.

Plasma protein binding of drug molecules can affect the efficiency of a drug, because the bound fraction is temporarily shielded from metabolism. On the other hand, only the unbound fraction exhibits pharmacological effects. The classification whether a compound is highly bounded ($\geq 90\%$ bound) to plasma proteins using the cutoff Bayesian score of -2.226 (obtained by minimizing the total number of false positives and false negatives) [57,58].

The results of ADME/Tox prediction of the benzoxazole (1) and oxazolo[4,5-*b*]pyridine (2) derivatives were shown in Table 5.

Human intestinal absorption (HIA) is defined as a percentage absorbed after oral administration. A well-absorbed compound is one that is absorbed at least 90% into the bloodstream in humans. The intestinal absorption model includes 95% and 99% confidence ellipses in the ADMET_PSA_{2D}, ADMET_AlogP₉₈ plane [54,59].

The ellipses define regions where well-absorbed compounds are expected to be found: 95% of well-absorbed compounds are expected to fall within the 95% ellipse, while 99% of well-absorbed compounds should fall within the 99% ellipse. In general, however, absorption tends

to drop off quite rapidly outside the 95% ellipse [54]. ADME plot of all benzoxazole (**1a-1r**) and oxazolo[4,5-*b*]pyridine (**2a-2i**) derivatives was given in Fig. 11.

2.6.3. Ames mutagenicity

The mutagenicity QSTR model of the TOPKAT program has been developed from compounds assayed according to the US EPA GeneTox protocol. According to this protocol, a chemical is tested against five strains of *Salmonella typhimurium*, namely: TA100, TA1535, TA1537, TA1538, and TA98, using the Histidine Reversion Assay [60].

Tests are performed both with and without S9 activation. A chemical is labeled a mutagen if a positive response, that is, a significant increase in number of reversions as compared to the background reversions, is observed against one or more strains, with or without S9 activation. A chemical is considered a non-mutagen if a negative response, that is, no significant increase in number of reversions as compared to the background reversions, is observed in all of these five bacterial strains with or without S9 activation. Therefore, when a query structure is assessed by TOPKAT to be a non-mutagen (computed probability of mutagenicity between 0.0 and 0.3), it indicates that, there is a high probability of the query chemical producing a negative response in the Histidine Reversion Assay, with or without S9 activation, against all of the five bacterial strains.

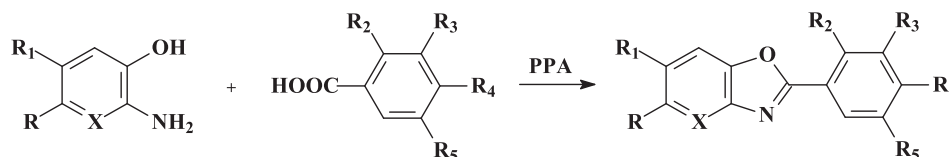
2.6.4. The developmental toxicity potential

The Developmental Toxicity Potential (DTP) Module of the TOPKAT package comprises three statistically significant and cross-validated quantitative structure–toxicity relationship (QSTR) models, and the data from which these models are derived. Each model applies to a specific class of chemicals. Molecular structure is the only input required to conduct a Developmental Toxicity Potential assessment. These discriminant models compute the probability of a submitted chemical structure being a developmental toxicant in the rat; a probability below 0.3 indicates no potential for developmental toxicity (NEG), and probability above 0.7 signifies developmental toxicity potential (POS). The probability range between 0.3 and 0.7 refers to the “indeterminate” zone (IND).

3. Results and discussion

3.1. Chemistry

The synthetic pathways for preparation of the target compounds listed in Table 1 are shown in Scheme 1. The synthesis of compounds (**1a-1r**, **2a-2i**) was performed by condensing of appropriate amine and suitable acids in polyphosphoric acid [34,61,62] in one step procedure as



X= CH, N; R=R₁=H, NO₂; R₂= H, CH₃, R₃= H, CH₃, SCH₃;
R₄= H, CH₃, CF₃, C(CH₃)₃, CH(CH₃)₂, C₄H₉; R₅= H, CH₃

Scheme 1. Reaction pathway of synthesized compounds (**1a-1r**, **2a-2i**).

seen in Scheme 1. In the present study, all the compounds are original except compounds **1a**, **1c**, **1j**, **1l**, **2a**, **2c-2h** [34–38].

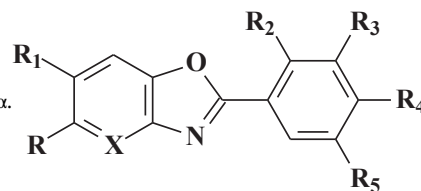
3.2. Biological evaluation

3.2.1. hTopo I and II α inhibitions

Inhibition of hTopo I and hTopo II α from the conversion of supercoiled pBR322 plasmid DNA by benzoxazole (**1**) and oxazolo[4,5-*b*]pyridine (**2**) derivatives were monitored using a relaxation assay. IC₅₀ values for inhibition of hTopo II α were in the micromolar range (Table 1). Clinically well-known Topo I and Topo II inhibitors CPT and etoposide, respectively were used as positive controls.

Most of the compounds did not show any activity against hTopo I enzyme. Only, **1a**, **1m**, **1o**, (2273, 3133, 2769 μ M, respectively) indicated less effect. Surprisingly, the effects on hTopo II α enzyme of these series either benzoxazole (**1**) and oxazolo[4,5-*b*]pyridines (**2**) exhibited very significant results that would allow further studies. Namely, all compounds showed more or less some activities between 2 μ M and over 3 mM with IC₅₀ values. Among the tested compounds only 5-nitro-2-(*p*-butylphenyl)benzoxazol (**1i**) and 2-(*p*-butylphenyl)oxazolo[4,5-*b*]pyridin (**2i**) displayed the most potency for hTopo II α with 2 μ M IC₅₀ value. These two small structures were found to be more effective than standard drug, etoposide (IC₅₀ value = 10 μ M). In parallel with earlier findings [31–33], *n*-butyl substitution on the *para* position of phenyl displayed lower IC₅₀ values (**1i**, **2i**) than the other substituents. According to previously CoMFA [32] and CoMSIA [33] studies we reported an electron-withdrawing and a hydrophilic group such as –NO₂ or –COOCH₃ at the 5 and/or 6 position of the heterocyclic ring system (benzoxazoles) increased the Topo II inhibitory activity. In addition, we also reported over there a hydrophobic and a bulky group at the *ortho* and *para* positions of the phenyl ring played a very important role for enhancing the Topo II inhibitory activity. In the present study, it has been observed that the most effective compounds were those that bearing *n*-butyl group at the *para* position of the phenyl ring. It is noticed that the *para* position is more important than others and, on this position, had to have more hydrophobic and steric substituent in order to achieve the best Topo II α inhibition effect. Even though the compound **1r** has *n*-butyl at the *para* location of phenyl ring, did not show good activity as much as **1i**. This result brings to mind a question of what the effect of the position of nitro group on the activity is. It can be considered that the position of 5 of benzoxazole ring is more substantial than 6 when we compare the position of nitro group. For increasing hTopo II α inhibition potent, 5-nitrobenzoxazole or oxazolo[4,5-*b*]pyridine as main pharmacophore cores can be used for further studies. On the other hand, the compounds **1k** (22 μ M), and **2d** (28 μ M) demonstrated moderate activity even if they showed lower potency than etoposide.

Table 1

IC₅₀ Values of benzoxazoles and oxazolo[4,5-*b*]pyridines versus hTopo I, hTopo II α .

| CompNo | X | R | R ₁ | R ₂ | R ₃ | R ₄ | R ₅ | Topo Inhibition IC ₅₀ (μM) | |
|--------|------|-----------------|-----------------|-----------------|------------------|-----------------|-----------------------------------|---------------------------------------|-------------------|
| | | | | | | | | hTopo I | hTopo II α |
| 1a | CH | NO ₂ | | | | | C(CH ₃) ₃ | 2273 | 188 |
| 1b | CH | NO ₂ | | | | | CH(CH ₃) ₂ | NE | 133 |
| 1c | CH | NO ₂ | | | | | CF ₃ | NE | 116 |
| 1d | CH | NO ₂ | | | SCH ₃ | | | NE | 652 |
| 1e | CH | NO ₂ | | CH ₃ | CH ₃ | | | NE | 376 |
| 1f | CH | NO ₂ | | CH ₃ | | CH ₃ | | NE | 191 |
| 1g | CH | NO ₂ | | CH ₃ | | | | NE | 884 |
| 1h | CH | NO ₂ | | | CH ₃ | | CH ₃ | NE | 263 |
| 1i | CH | NO ₂ | | | | | CH ₃ | NE | 2 |
| 1j | CH | | NO ₂ | | | | C ₄ H ₉ | NT | 2 |
| 1k | CH | | NO ₂ | | | | C(CH ₃) ₃ | NE | 657 |
| 1l | CH | | NO ₂ | | | | CH(CH ₃) ₂ | NE | 22 |
| 1m | CH | | NO ₂ | CH ₃ | CH ₃ | | CF ₃ | NE | 698 |
| 1n | CH | | NO ₂ | CH ₃ | | CH ₃ | | 3133 | 214 |
| 1o | CH | | NO ₂ | CH ₃ | | | | NE | 1043 |
| 1p | CH | | NO ₂ | | CH ₃ | | | 2769 | 143 |
| 1r | CH | | NO ₂ | | | | | CH ₃ | 3339 |
| 2a | N | | | | | | C ₄ H ₉ | NT | 483 |
| 2b | N | | | | | | C(CH ₃) ₃ | NE | > 3 mM |
| 2c | N | | | | | | CH(CH ₃) ₂ | NE | 7457 |
| 2d | N | | | | SCH ₃ | | CF ₃ | NE | 2909 |
| 2e | N | | | CH ₃ | CH ₃ | | | NE | 28 |
| 2f | N | | | CH ₃ | | CH ₃ | | NE | 1390 |
| 2g | N | | | | CH ₃ | | | NE | 277 |
| 2h | N | | | CH ₃ | | | | CH ₃ | 426 |
| 2i | N | | | | | | CH ₃ | NE | 315 |
| 2i | N | | | | | | C ₄ H ₉ | NT | 2 |
| PC* | CPT | | | | | | | 34 | NE |
| PC* | ETOP | | | | | | | NE | 10 |

*Positive control; CPT: Camptothecin, ETOP: Etoposide, NT: Not tested, NE: No effect.

3.2.1.1. SAR for hTopo II α . The results of structure-hTopo II α inhibition activity of the synthesized benzoxazoles and oxazolo[4,5-*b*]pyridines is summarized in Fig. 2.

Presence of an electron withdrawing group (–NO₂) in the 5th position has a positive effect on activity rather than the 6th position. At the same time oxazolo[4,5-*b*]pyridine core is slightly important than 6-nitrobenzoxazole for improving hTopo II α inhibition effect. Among the substituents on the phenyl ring located in the 2nd position, the *para* position shows higher activity, and gradually decreases towards the *meta* and *ortho* position. The fact that the substituent on the phenyl ring is an electron donating group increases the activity. While the straight alkyl chain located in *para* position of phenyl ring also enhances the activity, presence of a branched structure such as *tert*-butyl reduces activity due to steric shield.

3.2.2. Cytotoxic activity

In this study, the most active compounds (1i and 2i) were also tested using some of cancer lines such as HeLa (Human Epithelial Cervix Adenocarcinoma), WiDR (Human Epithelial Colorectal Adenocarcinoma), A549 (Human Lung Carcinoma), MCF7 (Human Breast Adenocarcinoma) for evaluating of the anti-tumor cytotoxicity (Table 2). However, 1i did not show any good activity on these cell lines. Compound 2i indicated 79,9 and 80,53 μM IC₅₀ values for HeLa and WiDR, respectively. Although these two compounds displayed very significant activity for hTopo II α , but they did not show satisfactory cytotoxicity on the tested cancer cell lines. It can be said that these compounds are not suit for HeLa, WiDR, A549, and MCF7. It can be considered that they have to test on different cancer cell lines.

When the cytotoxic effects of anticancer agents (e.g. CPT, etoposide,

etc.) routinely used as topoisomerase inhibitors on cancer cell lines are examined, it is seen that the effect can be quite different according to the cell line. A good example that we can give to this situation is the merbarone compound, which is routinely used as an hTopo II catalytic inhibitor. Although the IC₅₀ values of the effects of this compound on MCF7, HeLa, DU145 cells are 83.9, 62.3 and 18.9 μM, it is known to be much more effective in different types of cancer cell lines (MT-4 (T-cell Leukaemia) etc.) even at lower IC₅₀ concentrations (12 μM) [63,64].

The relaxation assay, in which we tested topoisomerase inhibition, is a cell-free system. However, in order to observe the same effect in the cell-dependent system, the first requirement is that the sufficient amount of the compound can enter the cell and reach the nucleus stably. It suggests that the reason why the high activity we detected in the cell-free system in our experiment could not affect the cell environment in the same way may be that the compounds could not enter the cell at sufficient concentrations.

In conclusion, in the light of these data we have obtained, the effects of compounds should be examined on different cell lines and possible problems with the cell pathways should be determined.

Table 2

IC₅₀ Values of compounds 1i and 2i versus some cancer cell lines.

| CompNo | In vitro Anticancer Activity IC ₅₀ (μM) | | | |
|--------|----------------------------------------------------|-------|-------|-------|
| | HeLa | WiDR | A549 | MCF7 |
| 1i | >100 | 100 | >100 | >100 |
| 2i | 79,9 | 80,53 | >100 | >100 |
| CPT | 5,27 | 2,50 | 0,809 | 1,959 |
| ETOP | 4,98 | 11,02 | 22,85 | 6,023 |

Table 3Docking results of the most active hTopo II α inhibitors.

| Compounds | Docking Score | Glide Score |
|-----------|---------------|-------------|
| 1i | -5.452 | -5.452 |
| 2i | -4.823 | -4.823 |
| Etoposide | -10.193 | -10.193 |

3.2.3. Molecular docking studies

The 3D molecular docking of the most active compounds (**1i**, **2i**) molecules on crystal structure of hTopo II α (PDB ID: **5GWK**) (Fig. 3a) was performed by using Schrödinger molecular modeling software (Schrödinger Release 2018–2, LLC, New York, NY, USA) [43,44] for the first time to evaluate the binding energies as well as their mode of interaction with the active site of the enzyme. To predict the binding

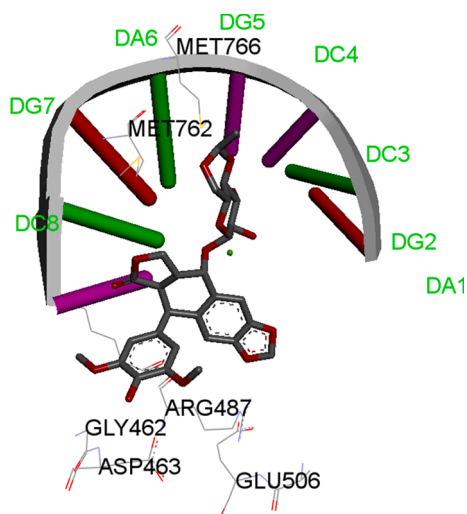


Fig. 4. Binding pocket with etoposide [65].

affinities and best alignment of the compounds at the active site of the enzyme, hydrogen bonds and π interactions formed with the surrounding amino acids and glide scores were used. All the results were shown in Table 3.

According to the docking results, compounds **2i** and **1i** showed strong interactions between one of the important active site residues, Arg487 and DNA similar to etoposide. When we look at the superposition of **2i** and etoposide, both have π interactions with Arg487 (Fig. 3b). Compounds **2i** revealed π - π stacking with DA12 and DG13, π -cation interaction with Arg487 (Fig. 3c); Structure **1i** revealed π - π stacking with DC8, DA12 and DG13, π -cation interaction with Arg487 (Fig. 3d).

3.2.4. Molecular dynamics simulations

We selected compounds **1i** and **2i** having the best hTopo II α inhibitory activity for the Molecular Dynamics (MD) simulations using AMBER. Human Topo II α (**5GWK**) in complex with DNA and etoposide from protein data bank was used for this study, as well. Molecular dynamics simulations between hTopo II α and etoposide were implemented Huang et al. [65] ALA505, GLU506, LYS489, ARG487, GLY462, ASP463, MET762, MET766 residues and DA6, DG5, DG2, DC3, DG4, bases were found in binding pocket (Fig. 4) [65].

For the analysis of binding profile for compounds **1i** and **2i** of MD simulations were implemented for 75 nsec. The plots of RMSD curves for complex are shown in Figs. 5 and 6. In there, blue line, green line, black line, and red line represent whole system, protein structure, DNA helix, compounds, respectively. Initial coordinates of the peptide, DNA and compound (Supporting Information) were taken as reference in RMSD computations. As seen in the Fig. 5, although compound **2i** was conformationally stabilized after 30 nsec of MD (red lines), the protein structure was stabilized after 65 nsec. This situation in the MD study indicates that the last 10 nsec of the MD curve can be used for understanding of the binding profile.

While compound **1i** conformationally is stabilized after 45 nsec of MD (red lines), the protein structure is stabilized after 65 nsec as seen in Fig. 6. It is pointed out that the last 10 nsec of the MD trajectory can be

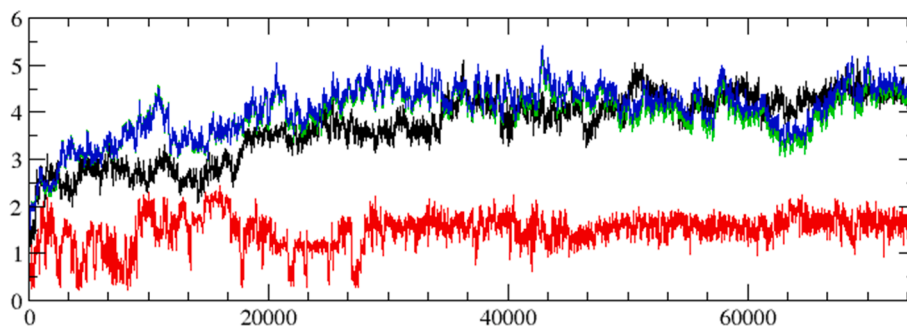


Fig. 5. RMSD curve for compound **2i** and protein complex (blue line refers to whole system; green line refers to protein structure; black line refers to DNA helix; red line refers to compound). (For interpretation of the references to colour in this figure legend, the reader is referred to the web version of this article.)

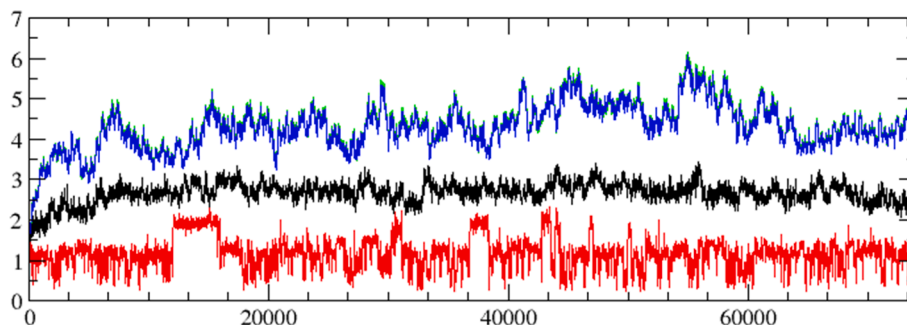


Fig. 6. RMSD curve for compound **1i** and protein complex.

utilized to understand of the binding profile.

Superposition of the X-ray structure of complex, PDB ID: 5GWK [45] with the last snapshot coordinates of system that was extracted from the 75 nsec MD trajectory, as shown in Fig. 7 Fig. 7A-B. This clearly indicates that the integrity of α -helical and β -pleated sheet structures throughout protein is mainly preserved after MD computation of compound 2i and hTopo II α complex. However, DNA helix twists on counterclockwise, protein structure shows a elastic recovery by the shrinking of the helix parts.

The integrity of α -helical and β -pleated sheet structures throughout protein is mainly preserved after MD computation of 1i and hTopo II α complex as well as 2i (see Fig. 8A–B). Besides, DNA helix protects its position, shrinking of the protein structure could be seen easily.

It was observed that 2-(*p*-butylphenyl)-5-nitrobenzoxazole (1i) mainly interacted with the binding pocket of protein through the last 30 nsec of MD trajectory. Nitro group of compound 1i interacted with the guanidinium group of ARG487 (Fig. 9). This hydrogen bond was protected for whole last 30 nsec.

2-(*p*-Butylphenyl)oxazolo[4,5-*b*]pyridine (2i) was also interacted with the binding pocket of protein through the last 10 ns of MD trajectory. Oxazole part of oxazolo[4,5-*b*]pyridine ring of 2i provides hydrogen bond acceptor points by both “O” and “N” atoms. While “O” of oxazole ring of 2i interacted with the amino group of residue GLU506, “N” formed hydrogen bond with DG5 of purine ring (Fig. 10). However,

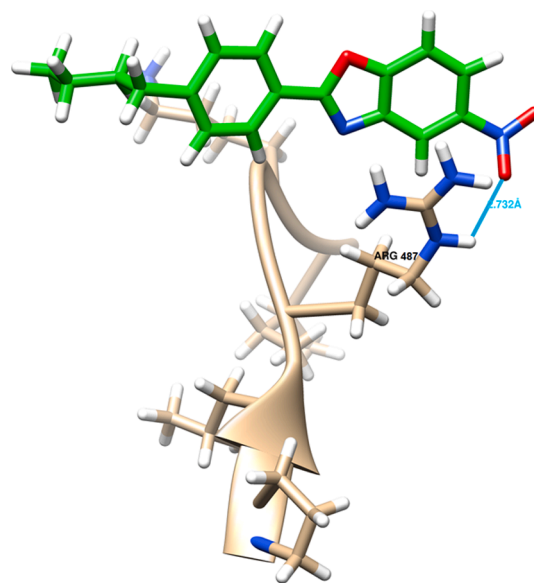


Fig. 9. Hydrogen bonding between ARG487 and 2-(*p*-butylphenyl)-5-nitrobenzoxazole (1i).

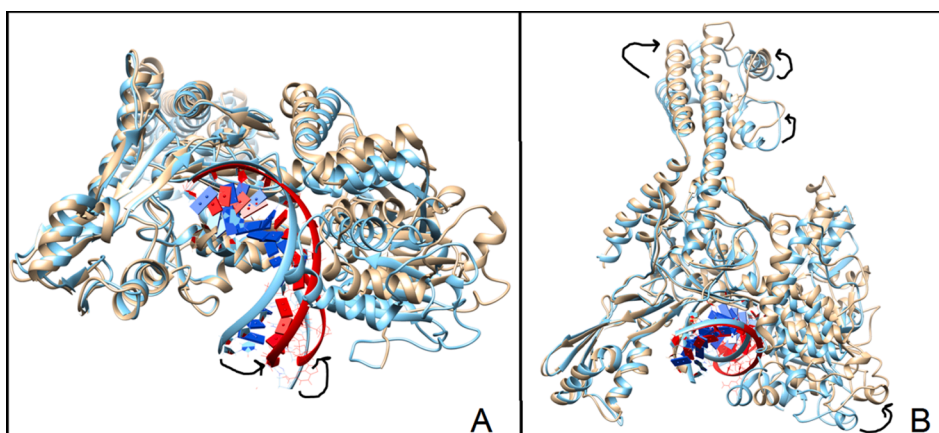


Fig. 7. Superposition of initial structure and the complex structure after 75 nsec MD. (A) Base view of the complex. DNA helix twisting counterclockwise. Blue helix shows initial coordinates, red helix shows the structure after MD. (B) Front view of complex. Shrinking on the helices was shown with arrows. Blue protein shows the initial coordinates. (For interpretation of the references to colour in this figure legend, the reader is referred to the web version of this article.)

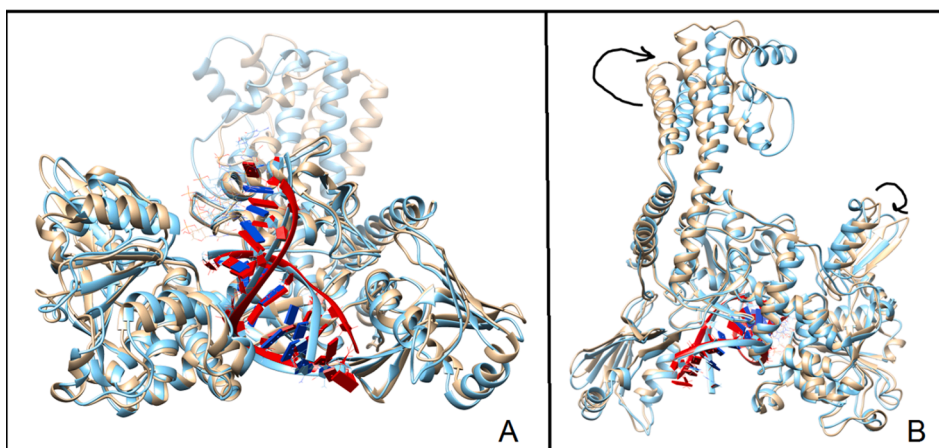


Fig. 8. Superposition of initial structure and the complex structure after 75 nsec MD. (A) Base view of the complex. DNA helix protects its position. Red helix shows initial coordinates, red helix shows the structure after MD. (B) Front view of complex. Shrinking on the helices was shown with arrows. Light brown protein shows the initial coordinates. (For interpretation of the references to colour in this figure legend, the reader is referred to the web version of this article.)

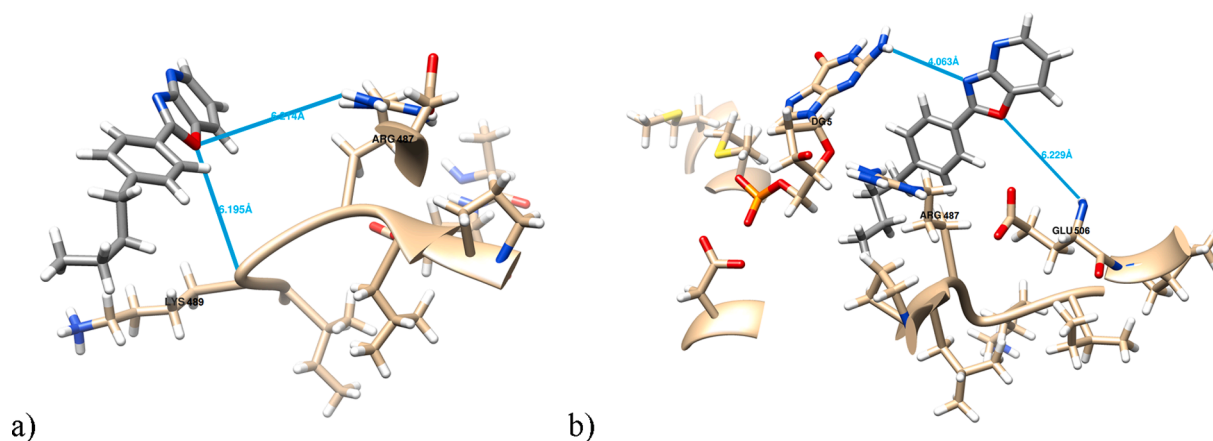


Fig. 10. (a) Hydrogen bonding between ARG487, LYS489 and 2-(p-butylphenyl) oxazolo[4,5-b]pyridine (**2i**) at the beginning of MD simulation. (b) Hydrogen bonding between GLU506, DG5 and **2i** at last 10 nsec of MD.

at the beginning of the MD simulation, compound **2i** had interacted with ARG487. It was seen that the compound **2i** formed two hydrogen bonds with GLU506 residue and DG5 base in the last 10 nsec of MD simulation. In here, it was noticed that GLU506 prevents the exit of **2i** from the binding groove of receptor. (Please refer to the link for the movement of **2i** in the [Supporting Information](#))

3.2.5. *In silico* ADME/Tox properties

Nowadays, *in silico* calculations have been came into prominence in order to minimize the unfavorable ADME/Tox properties and to ensure

that the newly developed drugs could have better properties [66]. *In silico* ADME calculations are extensively used for molecular modeling studies to understand structure–property relationships and to predict drug metabolism and pharmacokinetic properties [67].

In this study, the drug-likeness, molecular and ADME/Tox properties of all synthesized and tested compounds were calculated by using Discovery Studio 3.5 [47]. First of all, we screened the drug-likeness profiles of compounds in terms of their suitability to Lipinski [51] and Veber [52] rules. The data was given in Table 4. All compounds except **1i** and **1r** whose AlogP values slightly >5, were detected to be suitable

Table 4
Molecular properties of benzoxazoles (**1a–1r**) and oxazolo[4,5-b]pyridines (**2a–2i**),

| Comp. No | AlogP | MW | n_HBA | n_HBD | n_rot | n_ring | n_Ar | PSA_2D | n_vio. |
|-----------------|-------|---------|-------|-------|-------|--------|------|--------|--------|
| 1a | 4,575 | 296,321 | 3 | 0 | 3 | 3 | 3 | 66,638 | 0 |
| 1b | 4,369 | 282,294 | 3 | 0 | 3 | 3 | 3 | 66,638 | 0 |
| 1c | 4,117 | 308,212 | 3 | 0 | 3 | 3 | 3 | 66,638 | 0 |
| 1d | 3,716 | 286,306 | 4 | 0 | 3 | 3 | 3 | 66,638 | 0 |
| 1e | 4,147 | 268,267 | 3 | 0 | 2 | 3 | 3 | 66,638 | 0 |
| 1f | 4,147 | 268,267 | 3 | 0 | 2 | 3 | 3 | 66,638 | 0 |
| 1g | 4,147 | 268,267 | 3 | 0 | 2 | 3 | 3 | 66,638 | 0 |
| 1h | 4,147 | 268,267 | 3 | 0 | 2 | 3 | 3 | 66,638 | 0 |
| 1i | 5,029 | 296,321 | 3 | 0 | 5 | 3 | 3 | 66,638 | 1 |
| 1j | 4,575 | 296,321 | 3 | 0 | 3 | 3 | 3 | 66,638 | 0 |
| 1k | 4,369 | 282,294 | 3 | 0 | 3 | 3 | 3 | 66,638 | 0 |
| 1l | 4,117 | 308,212 | 3 | 0 | 3 | 3 | 3 | 66,638 | 0 |
| 1m | 4,147 | 268,267 | 3 | 0 | 2 | 3 | 3 | 66,638 | 0 |
| 1n | 4,147 | 268,267 | 3 | 0 | 2 | 3 | 3 | 66,638 | 0 |
| 1o | 4,147 | 268,267 | 3 | 0 | 2 | 3 | 3 | 66,638 | 0 |
| 1p | 4,147 | 268,267 | 3 | 0 | 2 | 3 | 3 | 66,638 | 0 |
| 1r | 5,029 | 296,321 | 3 | 0 | 5 | 3 | 3 | 66,638 | 1 |
| 2a | 3,726 | 252,311 | 2 | 0 | 2 | 3 | 3 | 35,076 | 0 |
| 2b | 3,519 | 238,284 | 2 | 0 | 2 | 3 | 3 | 35,076 | 0 |
| 2c | 3,268 | 264,203 | 2 | 0 | 2 | 3 | 3 | 35,076 | 0 |
| 2d | 2,867 | 242,296 | 3 | 0 | 2 | 3 | 3 | 35,076 | 0 |
| 2e | 3,298 | 224,258 | 2 | 0 | 1 | 3 | 3 | 35,076 | 0 |
| 2f | 3,298 | 224,258 | 2 | 0 | 1 | 3 | 3 | 35,076 | 0 |
| 2g | 3,298 | 224,258 | 2 | 0 | 1 | 3 | 3 | 35,076 | 0 |
| 2h | 3,298 | 224,258 | 2 | 0 | 1 | 3 | 3 | 35,076 | 0 |
| 2i | 4,18 | 252,311 | 2 | 0 | 4 | 3 | 3 | 35,076 | 0 |
| Lipinski's Rule | ≤5 | <500 | ≤10 | ≤5 | | | | | ≤1 |
| Veber Rule | | | ≤12 | | ≤10 | | | ≤140 | 0 |

AlogP: the log value of octanol–water partition coefficient,
MW: molecular weight.

n_HBA: number of hydrogen bond acceptor.

n_HBD: number of hydrogen bond donor.

n_rot: number of rotatable bonds.

n_ring: number of rings.

n_Ar: number of aromatic rings.

PSA_2D: 2D polar surface area.

n_vio.: violations from Lipinski's rule of five or Veber rules.

Table 5
ADME/Tox properties of synthesized compounds (1a-1r, 2a-2i).

| Comp. No | Sol. | BBB | Abs. Lev. | CYP2D6 | CYP2D6 Pred. | Hepatot. | Hepatot. Pred. | PPB | PPB Pred. | DTP Prob. | DTP Pred. | AMES Prob. | AMES Pred. |
|----------|--------|-------|-----------|-----------|--------------|-----------|----------------|---------|-----------|-----------|-----------|------------|------------|
| 1a | -5,981 | 0,206 | 0 | -4,50583 | false | 6,89242 | true | 10,2943 | true | 0,462518 | Non-Tox. | 0,204236 | Non-Mut. |
| 1b | -5,688 | 0,142 | 0 | -4,48847 | false | 8,08332 | true | 9,51438 | true | 0,428538 | Non-Tox. | 0,282564 | Non-Mut. |
| 1c | -5,621 | 0,064 | 0 | -1,37569 | false | 3,9971 | true | 11,2172 | true | 0,429121 | Non-Tox. | 0,162506 | Non-Mut. |
| 1d | -5,060 | -0,06 | 0 | -4,44524 | false | 7,51601 | true | 8,20364 | true | 0,478355 | Non-Tox. | 0,542507 | Non-Mut. |
| 1e | -5,591 | 0,073 | 0 | -4,89291 | false | 4,66038 | true | 7,38375 | true | 0,462383 | Non-Tox. | 0,594832 | Non-Mut. |
| 1f | -5,585 | 0,073 | 0 | -5,86512 | false | 4,64077 | true | 7,84808 | true | 0,453826 | Non-Tox. | 0,593382 | Non-Mut. |
| 1g | -5,59 | 0,073 | 0 | -5,66685 | false | 5,03583 | true | 6,7395 | true | 0,45066 | Non-Tox. | 0,635974 | Non-Mut. |
| 1h | -5,585 | 0,073 | 0 | -6,16644 | false | 5,92295 | true | 7,305 | true | 0,46448 | Non-Tox. | 0,578182 | Non-Mut. |
| 1i | -6,028 | 0,346 | 0 | -5,22693 | false | 7,06498 | true | 11,0665 | true | 0,515893 | Non-Tox. | 0,33227 | Non-Mut. |
| 1j | -5,981 | 0,206 | 0 | -4,1141 | false | 5,868 | true | 9,1346 | true | 0,447309 | Non-Tox. | 0,137759 | Non-Mut. |
| 1k | -5,688 | 0,142 | 0 | -4,09675 | false | 7,0589 | true | 8,3547 | true | 0,414559 | Non-Tox. | 0,202474 | Non-Mut. |
| 1l | -5,621 | 0,064 | 0 | -0,983972 | false | 2,97268 | true | 10,0575 | true | 0,41512 | Non-Tox. | 0,105731 | Non-Mut. |
| 1m | -5,591 | 0,073 | 0 | -4,50119 | false | 3,92563 | true | 6,57104 | true | 0,447179 | Non-Tox. | 0,542393 | Non-Mut. |
| 1n | -5,585 | 0,073 | 0 | -5,4734 | false | 3,90601 | true | 7,03537 | true | 0,438917 | Non-Tox. | 0,54077 | Non-Mut. |
| 1o | -5,590 | 0,073 | 0 | -5,27513 | false | 4,30108 | true | 5,92679 | true | 0,435863 | Non-Tox. | 0,588996 | Non-Mut. |
| 1p | -5,585 | 0,073 | 0 | -5,77472 | true | 4,89853 | true | 6,14533 | true | 0,449206 | Non-Tox. | 0,500051 | Non-Mut. |
| 1r | -6,028 | 0,346 | 0 | -4,83521 | false | 6,04056 | true | 9,90679 | true | 0,499128 | Non-Tox. | 0,246615 | Non-Mut. |
| 2a | -5,343 | 0,523 | 0 | -1,42132 | false | 2,73681 | true | 3,40257 | true | 0,440437 | Non-Tox. | 0,346366 | Non-Mut. |
| 2b | -5,034 | 0,46 | 0 | -1,49928 | false | 3,85068 | true | 2,45855 | true | 0,414299 | Non-Tox. | 0,431082 | Non-Mut. |
| 2c | -4,983 | 0,382 | 0 | 0,642698 | true | -0,114222 | true | 4,47375 | true | 0,387302 | Non-Tox. | 0,289392 | Non-Mut. |
| 2d | -4,386 | 0,258 | 0 | -2,23427 | false | 3,4907 | true | 1,33802 | true | 0,445249 | Non-Tox. | 0,611188 | Non-Mut. |
| 2e | -4,914 | 0,391 | 0 | -3,66074 | false | 1,54716 | true | 2,74554 | true | 0,42364 | Non-Tox. | 0,638715 | Non-Mut. |
| 2f | -4,909 | 0,391 | 0 | -4,63295 | false | 1,52755 | true | 3,20987 | true | 0,41587 | Non-Tox. | 0,651816 | Non-Mut. |
| 2g | -4,908 | 0,391 | 0 | -4,93428 | false | 2,23041 | true | 1,97287 | true | 0,425548 | Non-Tox. | 0,642121 | Non-Mut. |
| 2h | -4,913 | 0,391 | 0 | -4,43468 | false | 1,92261 | true | 2,10129 | true | 0,413003 | Non-Tox. | 0,674526 | Non-Mut. |
| 2i | -5,395 | 0,664 | 0 | -2,17439 | false | 2,31379 | true | 5,05187 | true | 0,460808 | Non-Tox. | 0,48933 | Non-Mut. |

Sol. (Aqueous Solubility): $\log(\text{Sw}) < -8.0$: Extremely low (0); $-8.0 < \log(\text{Sw}) < -6.0$: No, very low, but possible (1); $-6.0 < \log(\text{Sw}) < -4.0$: Yes, low (2); $-4.0 < \log(\text{Sw}) < -2.0$: Yes, good (3); $-2.0 < \log(\text{Sw}) < 0.0$: Yes, optimal (4); $0.0 < \log(\text{Sw}) < 2.0$: No, too soluble (5).

logBB (BBB): $\log\text{BB} \geq 0.7$: Very high penetrants (0); $0 \leq \log\text{BB} < 0.7$: High penetrants (1), $-0.52 < \log\text{BB} < 0$: Medium penetrants (2), $\log\text{BB} \leq -0.52$: Low penetrants (3).

Abs. Lev. (Absorption levels): 0:Good; 1:Moderate; 2:Poor; 3:Very Poor.

CYP2D6 binding: true: inhibition of CYP2D6; false: no inhibition; CYP2D6 Pred. (CYP2D6 Prediction).

Hepatot. (Hepatotoxicity): true: hepatotoxic; false: non-hepatotoxic; Hepatot. Pred. (Hepatotoxicity prediction).

PPB: true: binding to plasma protein, false: no binding; PPB Pred. (PPB prediction).

DTP: developmental toxicity potential. The probability below 0.3 indicates no potential for developmental toxicity (NEG), and probability above 0.7 signifies developmental toxicity potential (POS); DTP Prob. (DTP probability); DTP Pred. (DTP prediction); Non-Tox. (Non-Toxic).

AMES: The probability below 0.3 indicates non-mutagen (NEG), and probability above 0.7 signifies mutagen (POS); AMES Prob. (AMES probability); AMES Pred. (AMES prediction); Non-Mut. (Non-Mutagen).

according to Lipinski's rule of five and Veber rules.

The results of pharmacokinetic properties of the compounds were presented in Table 5. According to these data, it was noticed that ADME properties of tested benzoxazoles and oxazolo[4,5-*b*]pyridines were found to be very satisfactory. This study showed us that they had an acceptable solubility, a very good absorption level, and highly penetrant

to the blood-brain barrier. In ADME plot (Fig. 11) of all compounds were placed into the prediction confidence space (95% and 99%) for the Blood Brain Barrier Penetration and Human Intestinal Absorption models, especially oxazolo[4,5-*b*]pyridine derivatives (2a-2i) were located in the middle of prediction confidence ellipses. Besides all compounds tended to bind plasma proteins. CYP2D6 was not played a

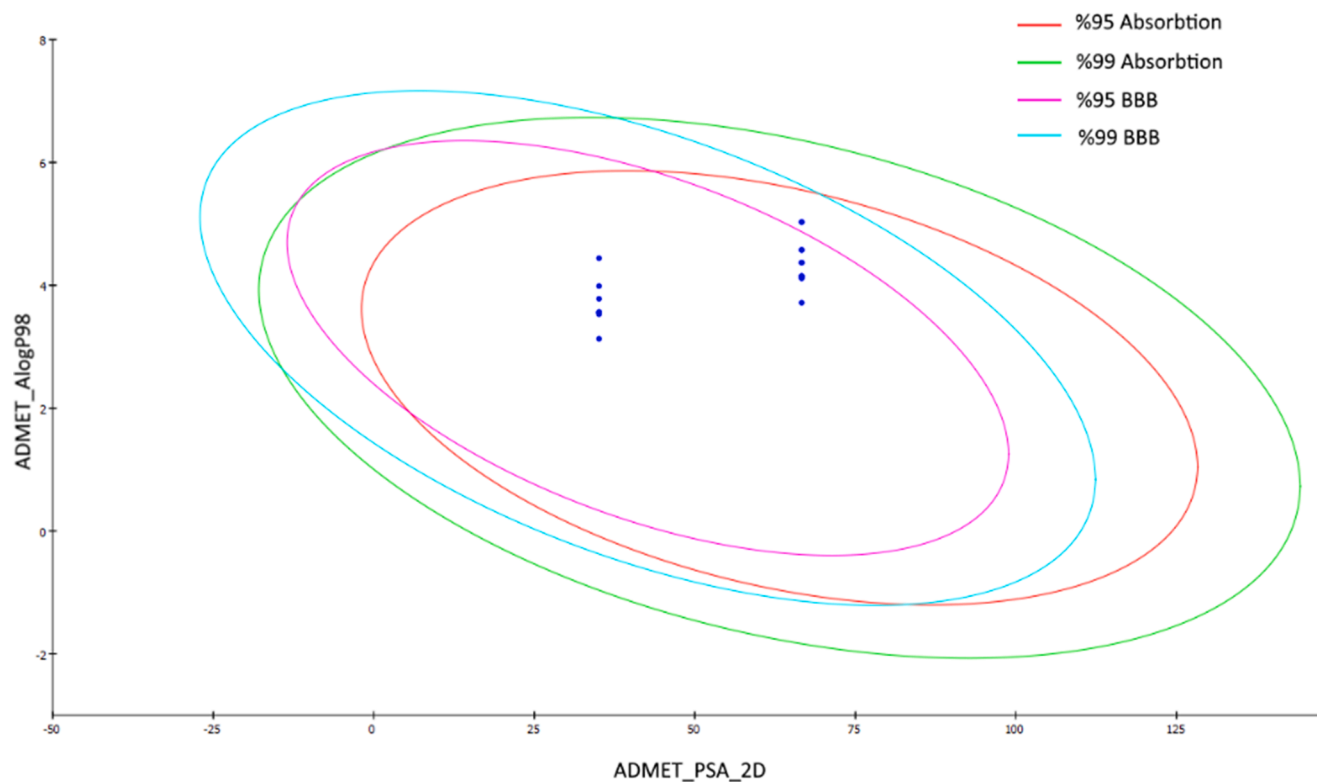


Fig. 11. Two dimensional ADME image for benzoxazoles (**1a-r**) and oxazolo[4,5-*b*]pyridines (**2a-i**).

role in metabolism of compounds except **1p** and **2c**. On the other hand, AMES and developmental toxicity potential (DTP) tests were calculated as toxicology tests and none of the compounds were predicted to exhibit mutagenicity and toxicity. Considering all these results, the synthesized compounds were thought to indicate good drug-likeness and pharmacokinetic properties, therefore, are estimated that they will exhibit good bioavailability.

4. Conclusion

In this study, we designed and synthesized a novel class 5(or 6)-nitro-2-(substitutedphenyl)benzoxazole (**1a-1r**) and 2-(substitutedphenyl)oxazolo[4,5-*b*]pyridine (**2a-2i**) compounds as candidate antitumor agents targeting human DNA topoisomerase enzymes (hTopo I and hTopo II α). None of the compounds indicated significant inhibition activity for hTopo I enzyme. Surprisingly, two original structures, 5-nitro-2-(4-butylphenyl)benzoxazole (**1i**) and 2-(4-butylphenyl)oxazolo[4,5-*b*]pyridine (**2i**), showed very significant effect on the hTopo II α with 2 μ M IC₅₀ value. Even these two small compounds displayed more activity than standard drug etoposide (10 μ M IC₅₀ value). These two molecules were also tested on some cancer cell lines such as HeLa, WiDR, A549, and MCF7. Unfortunately, they did not display any notable cytotoxicity. At this point, we can say that the compounds should be tried on different cancer cell lines. According to molecular dynamic simulations study, compound **2i** showed very close relationships with residue and nucleotide which are in the nearby of the active site of receptor, such as GLU506 and DG5, unlike the docking study. Compound **1i** formed hydrogen bond with ARG487 in the binding pocket similar as the molecular docking results. Moreover, ADME/Tox properties of all molecules were predicted using Discovery Studio 3.5 software programme. It can be noticed that the tested compounds were thought to indicate good drug-likeness and pharmacokinetic properties. Therefore, it can be estimated that they would exhibit good bioavailability. Considering all these results, especially original two small compounds **1i** and **2i** obtained from this study can be useful in designing of new potent inhibitors

of hTopo II α enzyme, as lead anticancer compounds.

Declaration of Competing Interest

The authors declare that they have no known competing financial interests or personal relationships that could have appeared to influence the work reported in this paper.

Acknowledgments

The Central Laboratory of the Faculty of Pharmacy, Ankara University supported the acquisition of the NMR, Mass spectra and elemental analyses in this work.

Appendix A. Supplementary material

Supplementary data to this article can be found online at <https://doi.org/10.1016/j.bioorg.2021.104913>.

References

- [1] H. Wang, M. Naghavi, C. Allen, R.M. Barber, Z.A. Bhutta, A. Carter, D.C. Casey, F. J. Charlson, A.Z. Chen, M.M. Coates, Global, regional, and national life expectancy, all-cause mortality, and cause-specific mortality for 249 causes of death, 1980–2015: a systematic analysis for the Global Burden of Disease Study 2015, *The Lancet* 388 (10053) (2016) 1459–1544.
- [2] WHO, Cancer Fact sheet N°297, World Health Organization, 2018.
- [3] D. Fabbro, D. Parkinson, A. Matter, Protein tyrosine kinase inhibitors: new treatment modalities? *Curr. Opin. Pharmacol.* 2 (4) (2002) 374–381.
- [4] M.A. Yildirim, K.-I. Goh, M.E. Cusick, A.-L. Barabási, M. Vidal, Drug–target network, *Nat. Biotechnol.* 25 (10) (2007) 1119–1126.
- [5] W.A. Denny, Chemotherapeutic Agents, in: D.J. Abraham (Ed.), *Burger's Medicinal Chemistry Drug Discovery*, John Wiley & Sons 2003, pp. 52.
- [6] T. Maxwell, A. Bates, *Topo 2008: DNA Topoisomerases in Biology and Medicine*, Oxford University Press, 2009.
- [7] D.B. Wigley, Structure and mechanism of DNA topoisomerases, *Ann. Rev. Biophys. Biomol. Struct.* 24 (1) (1995) 185–208.
- [8] J.C. Wang, DNA topoisomerases, *Ann. Rev. Biochem.* 65 (1) (1996) 635–692.

- [9] J.L. Nitiss, Investigating the biological functions of DNA topoisomerases in eukaryotic cells, *Biochimica et Biophysica Acta (BBA)-Gene Struct. Exp.* 1400 (1–3) (1998) 63–81.
- [10] Y. Pommier, Drugging topoisomerases: lessons and challenges, *ACS Chem. Biol.* 8 (1) (2013) 82–95.
- [11] J.M. Berger, S.J. Gamblin, S.C. Harrison, J.C. Wang, Structure and mechanism of DNA topoisomerase II, *Nature* 379 (6562) (1996) 225–232.
- [12] L. Stewart, M.R. Redinbo, X. Qiu, W.G. Hol, J.J. Champoux, A model for the mechanism of human topoisomerase I, *Science* 279 (5356) (1998) 1534–1541.
- [13] M.-A. Bjornsti, S.H. Kaufmann, Topoisomerases and cancer chemotherapy: recent advances and unanswered questions, *Frontiers Research* 8 (2019).
- [14] P. Forterre, S. Gribaldo, D. Gabelle, M.-C. Serre, Origin and evolution of DNA topoisomerases, *Biochimie* 89 (4) (2007) 427–446.
- [15] K. Buzun, A. Bielawska, K. Bielawski, A. Gornowicz, DNA topoisomerases as molecular targets for anticancer drugs, *J. Enzyme Inhib. Med. Chem.* 35 (1) (2020) 1781–1799.
- [16] E.L. Zechiedrich, K. Christiansen, A.H. Andersen, O. Westergaard, N. Osheroff, Double-stranded DNA cleavage/religation reaction of eukaryotic topoisomerase II: evidence for a nicked DNA intermediate, *Biochemistry* 28 (15) (1989) 6229–6236.
- [17] T. Syrovets, B. Büchele, E. Gedig, J.R. Slupsky, T. Simmet, Acetyl-boswellic acids are novel catalytic inhibitors of human topoisomerases I and II α , *Mol. Pharmacol.* 58 (1) (2000) 71–81.
- [18] M.E. Wall, M.C. Wani, C. Cook, K.H. Palmer, A.A. McPhail, G. Sim, Plant antitumor agents, *J. the Am. Chem. Soc.* 88 (16) (1966) 3888–3890.
- [19] Y. Kawato, H. Terasawa, 2 Recent Advances in the Medicinal Chemistry and Pharmacology of Camptothecin, in: *Prog. Med. Chem.*, Elsevier, 1997, pp. 69–109.
- [20] R. Garcia-Carbonero, J.G. Supko, Current perspectives on the clinical experience, pharmacology, and continued development of the camptothecins, *Clin. Cancer Res.* 8 (3) (2002) 641–661.
- [21] C.J. Thomas, N.J. Rahier, S.M. Hecht, Camptothecin: current perspectives, *Biorg. Med. Chem.* 12 (7) (2004) 1585–1604.
- [22] K.D. Bromberg, A.B. Burgin, N. Osheroff, A two-drug model for etoposide action against human topoisomerase II α , *J. Biol. Chem.* 278 (9) (2003) 7406–7412.
- [23] B.A. Teicher, Next generation topoisomerase I inhibitors: Rationale and biomarker strategies, *Biochem. Pharmacol.* 75 (6) (2008) 1262–1271.
- [24] A.K. Larsen, A.E. Escargueil, A. Skladanowski, Catalytic topoisomerase II inhibitors in cancer therapy, *Pharmacol. Ther.* 99 (2) (2003) 167–181.
- [25] E.M. Nelson, K.M. Tewey, L.F. Liu, Mechanism of antitumor drug action: poisoning of mammalian DNA topoisomerase II on DNA by 4'-O-acridinylamino-methanesulfon-m-anisidide, *Proc. Natl. Acad. Sci.* 81 (5) (1984) 1361–1365.
- [26] W. Beck, Y.-Y. Mo, U. Bhat, Cytotoxic Signalling by Inhibitors of DNA Topoisomerase II, Portland Press Ltd., 2001.
- [27] Y. Pommier, D. Kerrigan, R.E. Schwartz, J.A. Swack, A. McCurdy, Altered DNA topoisomerase II activity in Chinese hamster cells resistant to topoisomerase II inhibitors, *Cancer Res.* 46 (6) (1986) 3075–3081.
- [28] M.K. Danks, C.A. Schmidt, M.C. Cirtain, D.P. Suttle, W.T. Beck, Altered catalytic activity of and DNA cleavage by DNA topoisomerase II from human leukemic cells selected for resistance to VM-26, *Biochemistry* 27 (24) (1988) 8861–8869.
- [29] H. Lage, H. Helmbach, M. Dietel, D. Schadendorf, Modulation of DNA topoisomerase II activity and expression in melanoma cells with acquired drug resistance, *Br. J. Cancer* 82 (2) (2000) 488–491.
- [30] M. Hinds, K. Deisseroth, J. Mayes, E. Altschuler, R. Jansen, F.D. Ledley, L. A. Zwelling, Identification of a point mutation in the topoisomerase II gene from a human leukemia cell line containing an amsacrine-resistant form of topoisomerase II, *Cancer Res.* 51 (17) (1991) 4729–4731.
- [31] A. Pinar, P. Yurdakul, I. Yildiz, O. Temiz-Arpaci, N.L. Acan, E. Aki-Sener, I. Yalcin, Some fused heterocyclic compounds as eukaryotic topoisomerase II inhibitors, *Biochem. Biophys. Res. Commun.* 317 (2) (2004) 670–674.
- [32] O. Temiz-Arpaci, B. Tekiner-Gulbas, I. Yildiz, E. Aki-Sener, I. Yalcin, 3D-QSAR analysis on benzazole derivatives as eukaryotic topoisomerase II inhibitors by using comparative molecular field analysis method, *Biorg. Med. Chem.* 13 (23) (2005) 6354–6359.
- [33] B. Tekiner-Gulbas, O. Temiz-Arpaci, I. Yildiz, E. Aki-Sener, I. Yalcin, 3D-QSAR study on heterocyclic topoisomerase II inhibitors using CoMSIA, SAR QSAR Environ. Res. 17 (02) (2006) 121–132.
- [34] T. Ertan, I. Yildiz, B. Tekiner-Gulbas, K. Bolelli, O. Temiz-Arpaci, S. Ozkan, F. Kaynak, I. Yalcin, E. Aki, Synthesis, biological evaluation and 2D-QSAR analysis of benzoxazoles as antimicrobial agents, *Eur. J. Med. Chem.* 44 (2) (2009) 501–510.
- [35] T.-Y. Shen, R.L. Clark, A.A. Pessolano, B.E. Witzel, T.J. Lanza, Anti-inflammatory oxazole [4, 5-b] pyridines, Google Patents, 1977.
- [36] İ. Yalçın, E. Şener, T. Özden, Synthesis and Structure Elucidations of 2-(p-Substitutedphenyl) oxazolo (4, 5-b) pyridine Derivatives, *Ankara Üniversitesi Eczacılık Fakültesi Dergisi* 15 (1) (1985) 69–78.
- [37] T. Özden, S. Özden, E. Şener, İ. Yalçın, A. Akin, S. Yıldız, 5-Nitro-2-(p-süstitüefenil)-benzoksazol türevlerinin sentez, yapı açıklamaları ve mikrobiyolojik etkileri-III, *FABAD, Farm. Bil. Der* 12 (1987) 39–47.
- [38] G.K. Reen, A. Kumar, P. Sharma, In vitro and in silico evaluation of 2-(substituted phenyl) oxazolo [4, 5-b] pyridine derivatives as potential antibacterial agents, *Med. Chem. Res.* 26 (12) (2017) 3336–3344.
- [39] L. Stewart, J.J. Champoux, D.N.A. Topoisomerase, *Protocols: Volume II: Enzymology and Drugs (Methods in Molecular Biology)*, Humana Press, 2001.
- [40] E. Foto, Ç. Özen, F. Zilifdar, B. Tekiner-Gülbaş, İ. Yildız, E. Aki-Yalçın, N. Diril, İ. Yalçın, Benzoxazines as new human topoisomerase I inhibitors and potential poisons, *DARU J. Pharmac. Sci.* (2019) 1–9.
- [41] V. Vichai, K. Kirtikara, Sulforhodamine B colorimetric assay for cytotoxicity screening, *Nat. Protoc.* 1 (3) (2006) 1112–1116.
- [42] F. Zilifdar, E. Foto, T. Ertan-Bolelli, E. Aki-Yalçın, I. Yalcin, N. Diril, Biological evaluation and pharmacophore modeling of some benzoxazoles and their possible metabolites, *Arch. Pharm.* 351 (2) (2018) 1700265.
- [43] R.A. Friesner, R.B. Murphy, M.P. Repasky, L.L. Frye, J.R. Greenwood, T.A. Halgren, P.C. Sanschagrin, D.T. Mainz, Extra precision glide: Docking and scoring incorporating a model of hydrophobic enclosure for protein–ligand complexes, *J. Med. Chem.* 49 (21) (2006) 6177–6196.
- [44] R.A. Friesner, J.L. Banks, R.B. Murphy, T.A. Halgren, J.J. Klicic, D.T. Mainz, M. P. Repasky, E.H. Knoll, M. Shelley, J.K. Perry, Glide: a new approach for rapid, accurate docking and scoring. 1. Method and assessment of docking accuracy, *J. Med. Chem.* 47 (7) (2004) 1739–1749.
- [45] Y.-R. Wang, S.-F. Chen, C.-C. Wu, Y.-W. Liao, T.-S. Lin, K.-T. Liu, Y.-S. Chen, T.-K. Li, T.-C. Chien, N.-L. Chan, Producing irreversible topoisomerase II-mediated DNA breaks by site-specific Pt (II)-methionine coordination chemistry, *Nucleic Acids Res.* 45 (18) (2017) 10861–10871.
- [46] O. Trott, A.J. Olson, AutoDock Vina: improving the speed and accuracy of docking with a new scoring function, efficient optimization, and multithreading, *J. Comput. Chem.* 31 (2) (2010) 455–461.
- [47] Accelrys, *Discovery Studio*, San Diego, CA, 2012.
- [48] M.F. Sanner, Python: a programming language for software integration and development, *J. Mol. Graph. Model.* 17 (1) (1999) 57–61.
- [49] D. Case, T. Darden, T. Cheatham, C. Simmerling, J. Wang, R. Duke, R. Luo, K. Merz, D. Pearlman, M. Crowley, *AMBER 9* (San Francisco: University of California), 2006, 328 p.
- [50] E.F. Pettersen, T.D. Goddard, C.C. Huang, G.S. Couch, D.M. Greenblatt, E.C. Meng, T.E. Ferrin, UCSF Chimera—a visualization system for exploratory research and analysis, *J. Comput. Chem.* 25 (13) (2004) 1605–1612.
- [51] C.A. Lipinski, F. Lombardo, B.W. Dominy, P.J. Feeney, Experimental and computational approaches to estimate solubility and permeability in drug discovery and development settings, *Adv. Drug Del. Rev.* 23 (1–3) (1997) 3–25.
- [52] D.F. Veber, S.R. Johnson, H.-Y. Cheng, B.R. Smith, K.W. Ward, K.D. Kopple, Molecular properties that influence the oral bioavailability of drug candidates, *J. Med. Chem.* 45 (12) (2002) 2615–2623.
- [53] A. Cheng, K.M. Merz, Prediction of aqueous solubility of a diverse set of compounds using quantitative structure–property relationships, *J. Med. Chem.* 46 (17) (2003) 3572–3580.
- [54] W.J. Egan, G. Lauri, Prediction of intestinal permeability, *Adv. Drug Del. Rev.* 54 (3) (2002) 273–289.
- [55] R.G. Susnow, S.L. Dixon, Use of robust classification techniques for the prediction of human cytochrome P450 2D6 inhibition, *J. Chem. Inf. Comput. Sci.* 43 (4) (2003) 1308–1315.
- [56] A. Cheng, S.L. Dixon, In silico models for the prediction of dose-dependent human hepatotoxicity, *J. Comput. Aided Mol. Des.* 17 (12) (2003) 811–823.
- [57] S.L. Dixon, K.M. Merz, One-dimensional molecular representations and similarity calculations: methodology and validation, *J. Med. Chem.* 44 (23) (2001) 3795–3809.
- [58] J.R. Votano, M. Parham, L.M. Hall, L.H. Hall, L.B. Kier, S. Oloff, A. Tropsha, QSAR modeling of human serum protein binding with several modeling techniques utilizing structure–information representation, *J. Med. Chem.* 49 (24) (2006) 7169–7181.
- [59] W.J. Egan, K.M. Merz, J.J. Baldwin, Prediction of drug absorption using multivariate statistics, *J. Med. Chem.* 43 (21) (2000) 3867–3877.
- [60] J. Ashby, R.W. Tennant, Chemical structure, Salmonella mutagenicity and extent of carcinogenicity as indicators of genotoxic carcinogenesis among 222 chemicals tested in rodents by the US NCI/NTP, *Mutat. Res./Genetic Toxicol.* 204 (1) (1988) 17–115.
- [61] Y.-H. So, J.P. Heeschen, Mechanism of polyphosphoric acid and phosphorus pentoxide–methanesulfonic acid as synthetic reagents for benzoxazole formation, *J. Org. Chem.* 62 (11) (1997) 3552–3561.
- [62] T. Ertan-Bolelli, I. Yildiz, S. Ozgen-Ozgacar, Synthesis, molecular docking and antimicrobial evaluation of novel benzoxazole derivatives, *Med. Chem. Res.* 25 (4) (2016) 553–567.
- [63] J.A. Ortega, L. Riccardi, E. Minniti, M. Borgogno, J.M. Arencibia, M.L. Greco, A. Minarini, C. Sissi, M. De Vivo, Pharmacophore hybridization to discover novel topoisomerase II poisons with promising antiproliferative activity, *J. Med. Chem.* 61 (3) (2018) 1375–1379.
- [64] A. Spallarossa, C. Rotolo, C. Sissi, G. Marson, M.L. Greco, A. Ranise, P. La Colla, B. Busonera, R. Loddo, Further SAR studies on bicyclic basic merbarone analogues as potent antiproliferative agents, *Biorg. Med. Chem.* 21 (21) (2013) 6328–6336.
- [65] N.-L. Huang, J.-H. Lin, Recovery of the poisoned topoisomerase II for DNA religation: coordinated motion of the cleavage core revealed with the microsecond atomic simulation, *Nucleic Acids Res.* 43 (14) (2015) 6772–6786.
- [66] H. Yu, A. Adedoyin, ADME-Tox in drug discovery: integration of experimental and computational technologies, *Drug Discov. Today* 8 (18) (2003) 852–861.
- [67] F. Lombardo, P.V. Desai, R. Arimoto, K.E. Desino, H. Fischer, C.E. Keefer, C. Petersson, S. Winwarter, F. Broccatelli, In Silico Absorption, Distribution, Metabolism, Excretion, and Pharmacokinetics (ADME-PK): Utility and Best Practices. An Industry Perspective from the International Consortium for Innovation through Quality in Pharmaceutical Development: Miniperspective, *J. Med. Chem.* 60 (22) (2017) 9097–9113.